STANFORD GEOTHERMAL PROGRAM

Interdisciplinary Research in Engineering and Earth Sciences

Stanford University, Stanford, California

DISCLAIMER

SGP-TR-170

Relative Permeability Through Fractures

Gracel P. Diomampo

August 2001

Financial support was provided through the
Stanford Geothermal Program under
Department of Energy Grant No. DE-FG07-95ID13370
and No. DE-FG07-99ID13763,
and by the Department of Petroleum Engineering,
Stanford University

RELATIVE PERMEABILITY THROUGH FRACTURES

A REPORT SUBMITTED TO THE DEPARTMENT OF PETROLEUM ENGINEERING

OF STANFORD UNIVERSITY

IN PARTIAL FULFILLMENT OF THE REQUIREMENTS FOR THE DEGREE OF MASTER OF SCIENCE

By
Gracel P. Diomampo
August 2001

Abstract

The mechanism of two-phase flow through fractures is of importance in understanding many geologic processes. Currently, two-phase flow through fractures is still poorly understood. In this study, nitrogen-water experiments were done on both smooth and rough parallel plates to determine the governing flow mechanism for fractures and the appropriate methodology for data analysis. The experiments were done using a glass plate to allow visualization of flow. Digital video recording allowed instantaneous measurement of pressure, flow rate and saturation. Saturation was computed using image analysis techniques.

The experiments showed that gas and liquid phases flow through fractures in nonuniform separate channels. The localized channels change with time as each phase path undergoes continues breaking and reforming due to invasion of the other phase. The stability of the phase paths is dependent on liquid and gas flow rate ratio. This mechanism holds true for over a range of saturation for both smooth and rough fractures. In imbibition for rough-walled fractures, another mechanism similar to wave-like flow in pipes was also observed.

The data from the experiments were analyzed using Darcy's law and using the concept of friction factor and equivalent Reynold's number for two-phase flow. For both smooth- and rough-walled fractures a clear relationship between relative permeability and saturation was seen. The calculated relative permeability curves follow Corey-type behavior and can be modeled using Honarpour expressions. The sum of the relative permeabilities is not equal one, indicating phase interference. The equivalent homogenous single-phase approach did not give satisfactory representation of flow through fractures. The graphs of experimentally derived friction factor with the modified Reynold's number do not reveal a distinctive linear relationship.

Acknowledgments

This research was supported by the US Department of Energy under contract DE-FG07-99ID13763.

Contents

List of Tables

List of Figures

Chapter 1

1 Introduction

1.1 Theoretical Background

Multiphase flow in fractures is an important field of study for areas such as geothermal industry, oil recovery, isolation of nuclear and toxic waste in geological formations. At present, the governing flow mechanism for multiphase flow in fracture is still undetermined. There are two approaches commonly used in modeling multiphase flow in fractures, the porous medium approach and the equivalent homogeneous single-phase approach.

The porous medium approach treats fractures as connected two-dimensional porous media. In this model, a pore space occupied by one phase is not available for flow for the other phase. A phase can move from one position to another only upon establishing a continuous flow path for itself. As in porous media, the competition for pore occupancy is described by relative permeability and governed by Darcy's law. Darcy's law for single-phase liquid flow is:

$$q_l = \frac{k_{abs}(p_i - p_o)}{\mu_l L} \tag{1.1}$$

where subscript l stands for the liquid phase, i for inlet and o for outlet; μ, p, L, q, k_{abs} are the viscosity, pressure, fracture length, Darcy flow velocity and absolute permeability respectively. The Darcy flow velocity is equal to

$$q = \frac{Q}{bw} \tag{1.2}$$

with Q as the volumetric flow rate, b the fracture aperture and w as the fracture width. Absolute permeability of the fracture is a function only of the fracture aperture (Witherspoon et al., 1980) as described in the cubic law

$$k_{abs} = \frac{b^2}{12} \tag{1.3}$$

For liquid phase in two-phase flow, Eqn. (1.1) becomes

$$q_l = \frac{k_{abs} k_{rl} (p_i - p_o)}{\mu_l L} \tag{1.4}$$

where k_{rl} is the relative permeability of the liquid phase.

Similarly, Darcy's law derived for single-phase isothermal gas flow in porous media (Scheidegger, 1974) is

$$q_g = \frac{k_{abs} (p_i^2 - p_o^2)}{2\mu_g L p_o} \tag{1.5}$$

with the subscript g pertaining to the gas phase.

In two-phase flow, Eqn. (1.5) becomes

$$q_g = \frac{k_{abs} k_{rg} (p_i^2 - p_o^2)}{2\mu_g L p_o} \tag{1.6}$$

with k_{rg} as the gas relative permeability. The sum of the k_{rl} and k_{rg} indicates the extent of phase interference. A sum of relative permeabilities equal to one means the absence of phase interference. Physically this implies each phase flows in its own path without impeding the flow of the other. The lower is the sum of the relative permeabilities from unity the greater is the phase interference.

Relative permeability functions are usually taken to be dependent on phase saturation. The two most commonly used expression for relative permeability for homogeneous porous media are the X-curve and Corey curve (Corey, 1954). The X-curve describes relative permeability as a linear function of saturation

$$k_{rl} = S_l \tag{1.7}$$

$$k_{rg} = S_g \tag{1.8}$$

where S_l and S_g are the liquid and gas saturation respectively. The Corey curve relates relative permeability to the irreducible or residual liquid and gas saturation, S_{rl} and S_{rg}

$$k_{rl} = S^{*4} \tag{1.9}$$

$$k_{rg} = (1 - S^*)^2 (1 - S^{*2}) \tag{1.10}$$

$$S^* = (S_l - S_{rl})/(1 - S_{rl} - S_{rg}) \tag{1.11}$$

The equivalent homogeneous single-phase approach treats flow through fracture as a limiting case of flow through pipes. In this model, phase velocities in a fracture are equal and capillary forces are negligible. A continuous flow path is not required for movement of each phase. A phase can be carried along by one phase as bubbles, slug or other complex structures. As in pipes, flow can be described by the concept of friction factors and using averaged properties (Fourar et al., 1993)

$$(p_i - p_o) = \frac{\Pi f \rho_m V_m^2}{2A} \tag{1.12}$$

where Π is the fracture perimeter, A is the cross sectional area to flow, ρ_m average density and V_m as average flow velocity. The average density is described by

$$\rho_m = \frac{\rho_g Q_g + \rho_l Q_l}{Q_g + Q_l} \tag{1.13}$$

The average flow velocity is equal to

$$V_m = \frac{Q_g + Q_l}{A} \tag{1.14}$$

The friction factor, f, is derived empirically as a function of the averaged Reynolds number calculated by

$$N_{\mathrm{Re}} = \frac{2bV_m\rho_m}{\mu_m} \tag{1.15}$$

with μ_m as average viscosity

$$\mu_m = \frac{\mu_g Q_g + \mu_l Q_l}{Q_g + Q_l} \tag{1.16}$$

There are several expressions used to relate friction factor and Reynold's number. The commonly used one for flow through fracture is the generalized Blasium form (Lockhart and Martinelli, 1949):

$$f = \frac{C}{N_{\mathrm{Re}}^n} \tag{1.17}$$

with C and n as constants derived from experimental data.

The validity of the two models for multiphase flow through fractures is still uncertain.

1.2 Literature Review

Only a few published data are available for two-phase flow in fractures. Most of the studies have been done for air-water or for water-oil systems. Earliest is Romm's (1966) experiment with kerosene and water through an artificial parallel-plate fracture lined with strips of polyethylene or waxed paper. Romm found a linear relationship between permeability and saturation, $S_w = k_{rw}$, $S_{nw} = k_{rnw}$ such that $k_{rw}+k_{rnw} = 1$. Fourar et al. (1993) artificially roughened glass plates with beads and flowed air-water between them. Fourar and Borries (1995) did similar experiments using smooth glass plates and clay bricks. Both studies observed flow structures like bubble, annular and fingering bubbles comparable to flow in pipes and depicted flow in fractures to be better correlated using the equivalent homogeneous single-phase model. Pan et al. (1996) observed the identical flow structures in their experiment with oil-water systems. They observed that a discontinuous phase can flow as discrete units along with the other phase. Pan et al. (1996) also found their experimental pressure drop to be better predicted by homogenous single-phase model. All of these experiments show significant phase interference at intermediate saturations.

Pruess and Tsang (1990) conducted numerical simulation for flow through rough-walled fractures. They modeled fractures as two dimensional porous media with apertures varying with position. Their study shows the sum of the relative permeabilities is less than 1, residual saturation of the nonwetting phase is large and phase interference is greatly dependent on the presence or absence of spatial correlation of aperture in the direction of flow. Persoff et al. (1991) did experiments on gas and water flow through rough-walled fractures using transparent casts of natural fractured rocks. The experiment showed strong phase interference similar to the flow in porous media. The relative permeability data of Persoff (1991) and Persoff and Pruess (1995) for flow through rough-walled fractures were compared in Horne et al. (2000) against commonly used relative permeability relations for porous media, the X-curve and Corey curve as shown in Figure 1.1.

In both experiments of Persoff (1991) and Persoff and Pruess (1995), flow of a phase is characterized by having a localized continuous flow path that is undergoing blocking and unblocking by the other phase. Recent parallel plate experiment by Su et al. (1999) illustrates the same flow mechanism of intermittent localized fluid flow. Kneafsy and Pruess (1998) observed similar intermittent flow in their experiments with pentane through various parallel plate models made from glass, sandblasted glass or transparent fracture replicas. These observations are contrary to the findings of Fourar et al. (1993), Fourar and Bories (1995), and Pan et al. (1996).

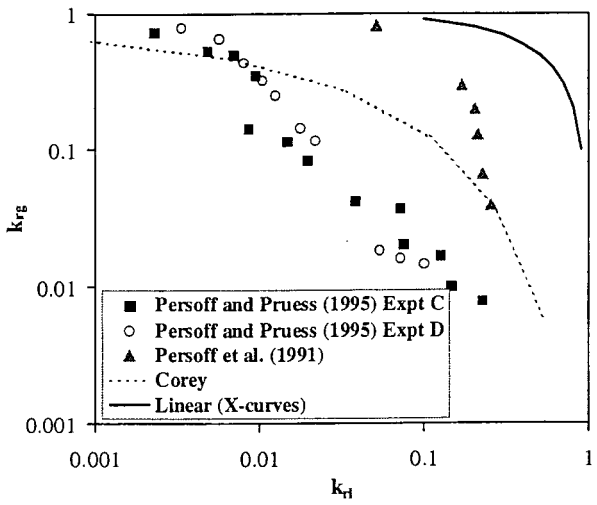

Figure 1.1 Measurement of air-water relative permeabilities in rough-walleded fractures (graph from Horne et al. 2000).

Presently, the mechanism of flow and the characteristic behavior of relative permeability in fractures are still undetermined. Issues such as whether a discontinuous phase can travel as discrete units carried along by another phase or will be trapped as residual saturation as in porous medium are unresolved. The question of phase interference i.e. is the relative permeability curve against saturation an X-curve, Corey or some other function is still unanswered. The main objective of this study is to contribute to the resolution of these issues.

Chapter 2

2 Experimental Methodology

This study conducted of experiments in smooth- and rough-walled fractures. The smooth-walled fracture experiment was done by flowing nitrogen and water in between glass and aluminum plates. The rough-walled fracture experiment was done with nitrogen-water flowing through a wire mesh inserted in between glass and aluminum. The nitrogen-water system was chosen mainly because of its simplicity since it can be done at room temperature and volume changes due to compressibility and solubility are negligible. The system does not have the complication of phase change. The nitrogen-water experiments will aid in establishing a reliable methodology for future study of flow characterization and permeability calculation for more complex systems such as steam-water flow.

2.1 Fracture Apparatus Description

The fracture apparatus consists of a smooth glass plate on top of an aluminum plate. The whole apparatus is confined by another metal frame bolted to the bottom plate. This was done to improve the seal and to prevent deformation of the glass due to system pressure. The metal frame has several windows and a mirror attached to it for flow visualization. (See Figure 2.1 and Figure 2.2)

An o-ring (Viton 1/8" thick #2-272) was placed in between the glass and aluminum plates as seal (see orange color lining in Figure 2.2). Placing this o-ring in the channel is not enough to provide a good seal because the channel was custom made in width and length. Thinly cut rubber sheets were placed at the outer boundary to push the o-ring to the sides of the aluminum plate. These provided excellent seal when compressed with the glass and metal frame. Since the o-ring is cylindrical in shape and the aluminum plate is rectangular, there will be a narrow channel in between the o-ring and the plate when squeezed together. A thin lining of copper based adhesive (Permatex Ultra Copper) was applied to minimize this channel. It is important to eliminate this channel for it serves as an easy conduit for the fluid to pass through instead of the fracture.

The phases enter the fracture through two separate canals. Each canal has several ports drilled in a way that they align on the surface (see Figure 2.1). The surface of the fracture apparatus was designed such that there is a 12" by 4" space available for flow. Throughout this flow area, tiny temperature ports the size of needles were drilled. Needle-size ports were drilled so as to minimize surface discontinuity. A pressure port was drilled at each end of the flow path. The two-phase fluid exits through a single outlet.

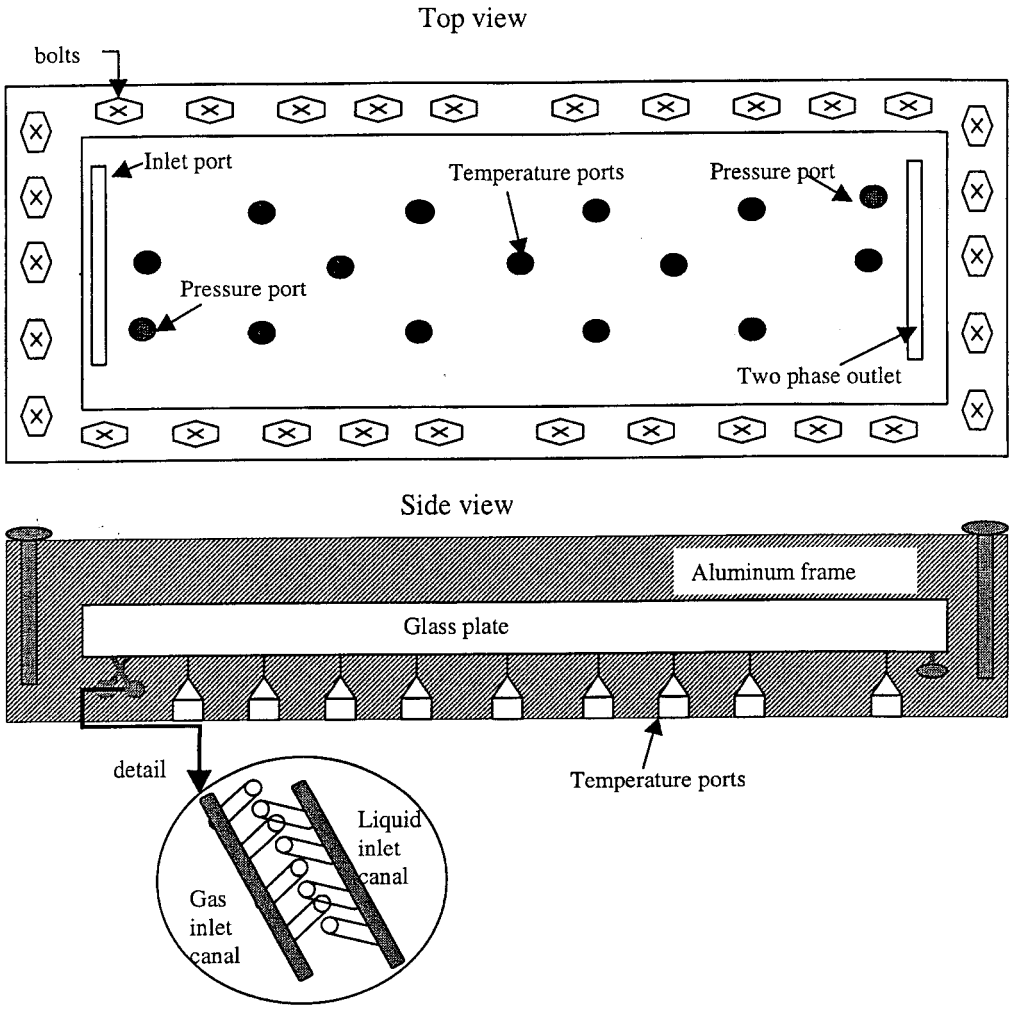

Figure 2.1 Schematic diagram of fracture apparatus.

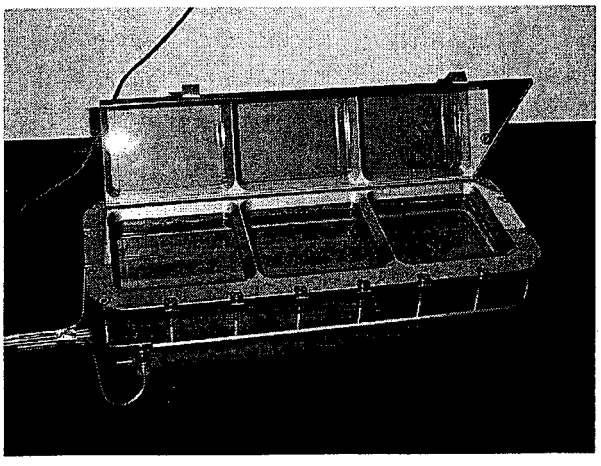

Figure 2.2 Picture of fracture apparatus.

2.2 Control and Measurement Techniques

There are two canals available for input of gas and liquid. The options to input nitrogen and water as separate streams or as mixed fluid in a single stream were tried. It was found that mixing the gas and water prior to input caused no significant improvement in fluid distribution. Thus, the gas and water streams were injected separately for simplicity, ease of flow rate control and inlet pressure reading.

Gas injection was controlled through a flow regulator (Matheson Flow Controller Model 8270). The gas regulator is connected to a gas meter (Matheson Flow Meter model 8170) that gives out a digital display. For water, a meter pump (Constameter pump model III) controls the rate of injection. Distilled deaerated water was used as injection fluid. Red dye was dissolved in the water for better phase identification.

Nitrogen and water enters at the far left of the apparatus. Both phases flow in between the glass and aluminum plate and exit at the far right through a single channel. Attached to the exit is a cross of larger diameter that enables the separation of the phases for outlet pressure measurement. Figure 2.3 is a schematic diagram of this configuration.

Low capacity differential transducers were used to measure the gas phase pressure drop, liquid phase pressure drop and the gas-phase outlet pressure. The liquid differential transducer (Celesco Transducer Model CD 10D range 0-5psi) is attached to the input water stream and to the bottom of the cross separating the phases at the outlet. The gas differential transducer (Celesco Transducer Model CD 10 D range 0-5psi) is connected to the nitrogen inlet and to the top of the cross separator. Another gas transducer (Celesco Transducer Model CD 10D range 0-0.5psi) is attached to the top of the cross separator. This last transducer measures the outlet pressure of the gas. These transducers send electrical signals to a Labview program designed to record pressure data at user specified time interval. See Figure 2.3.

Experience showed that these fracture experiments are unsteady state by nature. At a single gas-water input ratio, there is significant pressure fluctuations accompanied by saturation changes and change in gas flow rate (see Section 3.1.1). The water flow rate is considered constant since it is injected by meter pump. Due to this unsteady nature, data acquisition then requires gathering of instantaneous pressure, flow rate and saturation data.

Instantaneous data gathering was accomplished by the use of a digital video camera. Video shots were taken of the pressure, flow rate and saturation data displayed all at the same time. The pressure data were displayed by voltmeters attached to each transducer outlet. The digital output of the gas meter displays the gas flow rate. The saturation was taken from the image of the whole flow area of the fracture. Still images were then taken from the recorded video film. The data gathered from the video was connected with the Labview data through the time read from a digital clock recorded along with the other data. Figure 2.4 shows a typical video image taken from the experiments. See also Figure 2.3.

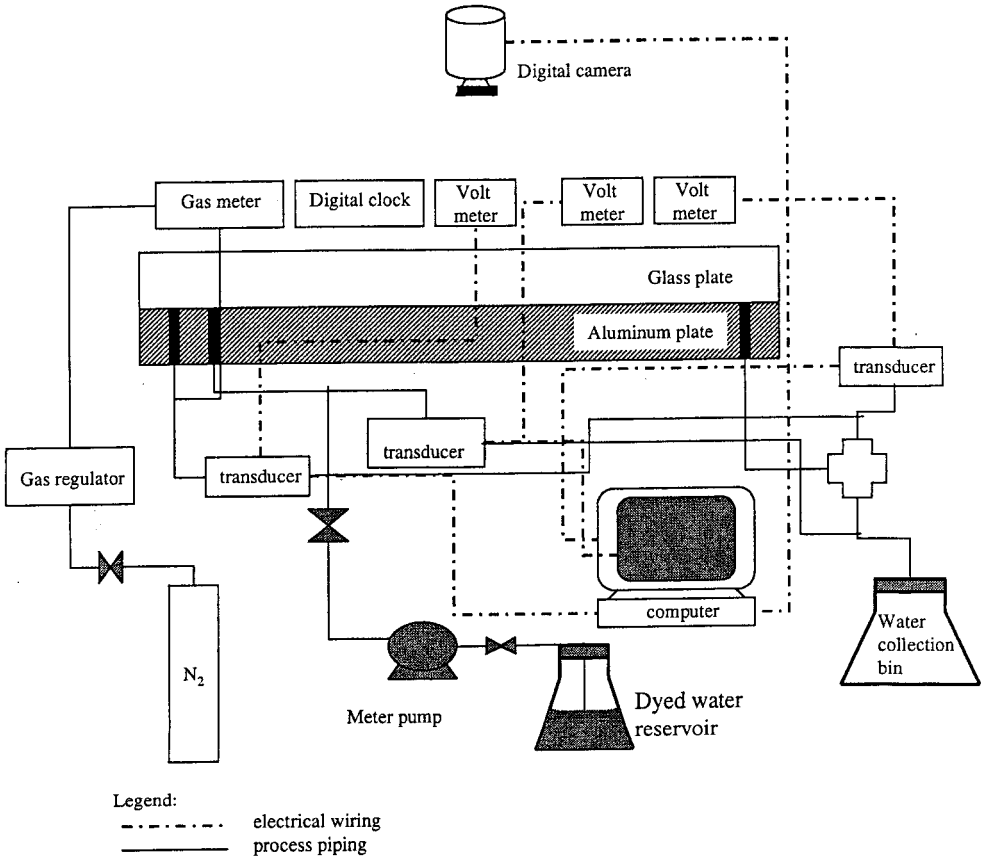

Figure 2.3 Process flow diagram for nitrogen-water experiment.

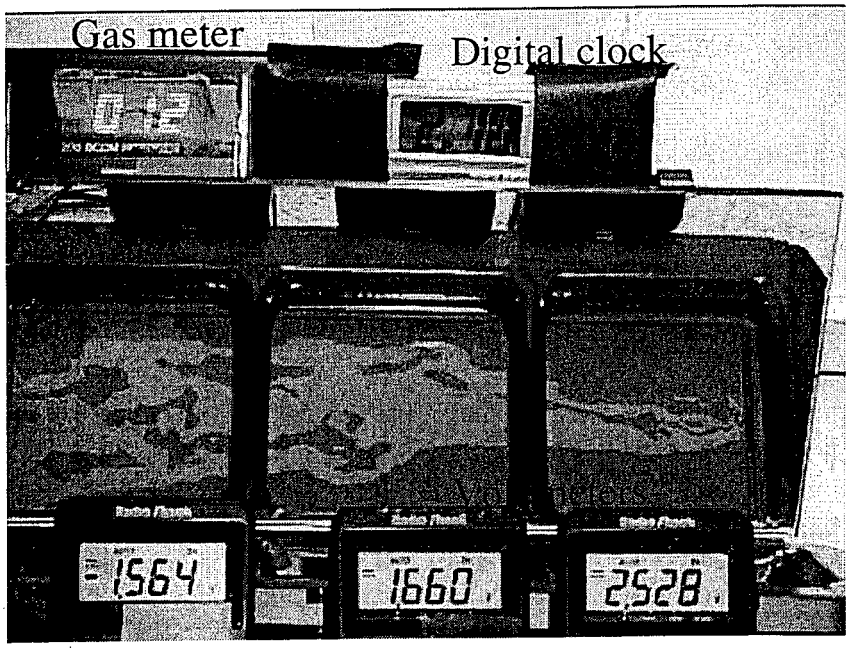

Figure 2.4 Sample video image taken for nitrogen-water runs.

Drainage and imbibition experiments were done for smooth- and for rough-walled fractures. The glass against the aluminum plate represented the smooth-walled fracture while the rough-walled was achieved by inserting a wire mesh between the glass and aluminum plate. The wire mesh is made from 0.00065" (0.0026cm) diameter stainless steel wire and has 30x30 mesh size. For both the rough- and smooth-walled fracture configurations, stainless steel shims were inserted at the perimeter of the flow area in between the glass and aluminum plate. The shims are 0.003" (0.0076cm) thick.

Drainage experiments were performed first. To start, the fracture was fully saturated with water. Unlike in porous media, parallel plates can be easily saturated with water if the aperture is small enough. Full saturation is achieved simply by flowing water at slow rate into the completely dried apparatus. This approach was used for both the smooth- and rough-walled configurations. The drainage experiment proceeded with the water injected at a constant rate and gas rate increased incrementally. If saturation change was not evident, then both the gas and the water rate were changed. The reverse was done for imbibition. At a specific gas-water ratio, the experiment was made to run for several minutes (usually 30 minutes) or up to a time when the pressure change was minimal or when pressure fluctuations seemed to be in certain range before taking video record.

2.3 Saturation Measurement

From the still image of the fracture flow shown in Figure 2.4, saturation was computed by measuring the area that each phase occupied. The photographs were processed in a Matlab program. The program first cuts the photograph to display just the image of the flow area. Using this cut image, the program does quadratic discriminant analysis to group the pixels of the picture into three groups: the water phase, gas phase and the frame. The grouping is based on color differences. Saturation is calculated as total pixels of liquid group over the sum of the gas and liquid group. Figure 2.5 is a comparison of the gray scaled image produced by the program and the original cut photograph from the digital camera. The accuracy of the program in calculating the saturation can be related to the similarity in details of the gray scale image to the true image. From the figure, it can be said that the program has reasonable accuracy. A copy of the Matlab program described here is attached in Appendix A.

Pan et al. (1996) also used this technique for measurement of saturation. Their study noted that the sources of error in this technique were the quality of the photographs and the water film adsorbed on the surfaces of the plates with the latter being of minimal effect. Good quality photographs are the ones with clear distinction between the gas and liquid phase. The use of dyed liquid enhanced visualization of phase boundaries. Good lighting is also necessary so that the colors in the image come out clearly. The lighting should also be positioned in a way that it does not produce shadow on the flow area. The program will mistakenly take the shadow as liquid phase even if there is gas. The light should be not too bright or focused too directly on the image to prevent reflection. Reflection will cast a white background on the picture. This will be taken automatically by the program as gaseous phase. In the experiment, good lighting was obtained by

taking the picture in the dark with lamps directed on the white ceiling to create adequate lighting on the apparatus.

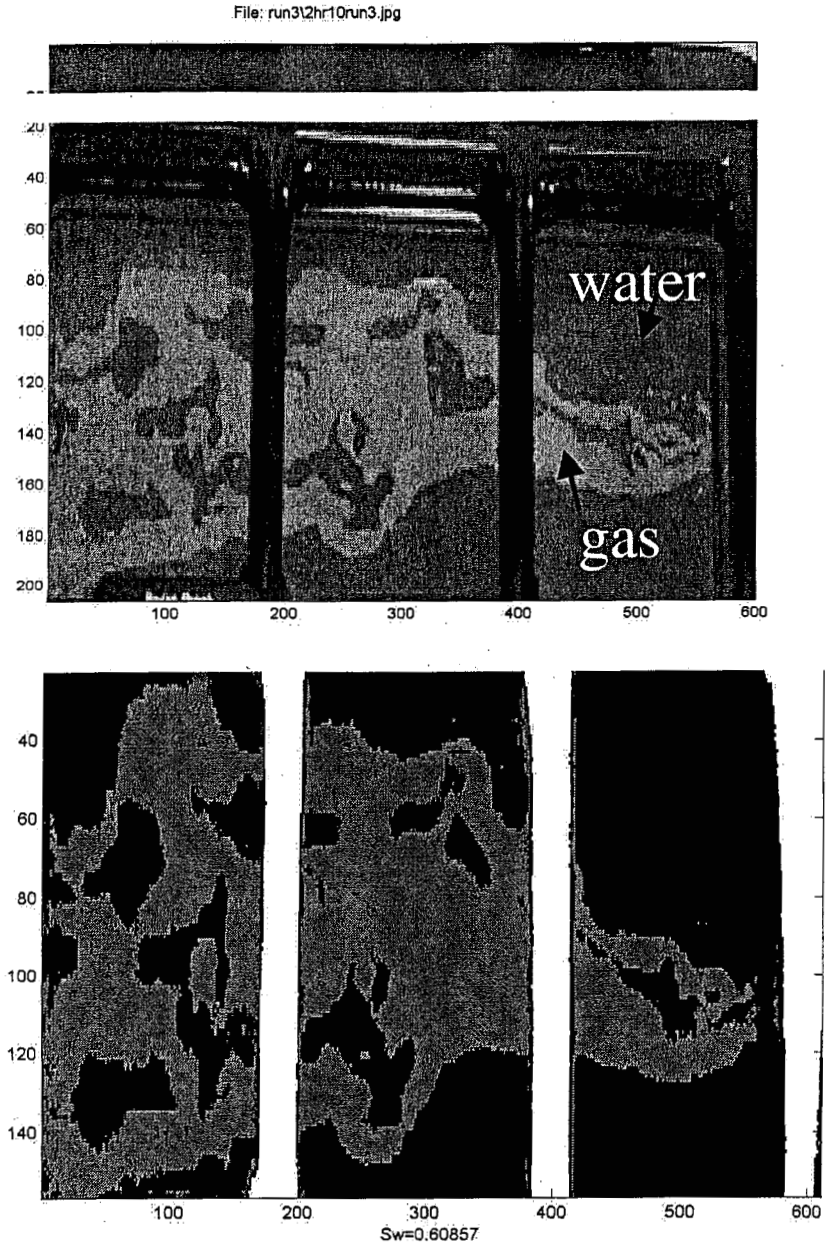

Figure 2.5 Comparison between the true color image of the fracture flow and gray scale image from Matlab program used in measuring saturation.

Chapter 3

3 Results and Discussion

3.1 Smooth-walled Fracture Experiments

3.1.1 Observed Flow Mechanism

One dominant flow mechanism was observed in the smooth-walled fracture experiment. Each phase travels through the fracture by forming a localized continuous flow path. This flow path is unstable as the other phase constantly blocks and unblocks certain points in the path.

For example in the drainage experiment, the gas forms its own flow path through the liquid-dominated fracture. This flow path undergoes continuous snapping and reforming due to the invasion of water. This blocking and unblocking of flow path causes continuous pressure fluctuations throughout the experiment even at a constant gas-water ratio. Figure 3.1 shows the pressure fluctuations and the corresponding events observed. Snap shot images of the flow at these times are seen in Figure 3.2. These pictures were taken at a gas rate of 19 cc/min and water rate of 8.5 cc/min. It was observed that the lower pressure drop corresponds to the time when gas is establishing its channel (see time 2:14 p.m. in Figure 3.1 and Figure 3.2). Upon establishing a complete path, gas is able to rush through the fracture length. This causes an increase in the gas pressure drop. As the gas surges, there is more space for water to come through the fracture. Water invades the gas channel (see time 2:16 p.m. in Figure 3.1 and Figure 3.2). As water breaks through there is an increase in liquid phase pressure drop. These are the pressure peaks seen in Figure 3.1. The cycle continues with the gas forming its pathway and water invading it (see time 2:17 p.m. and 2:18 p.m. in Figure 3.1 and Figure 3.2).

This flow mechanism of moving through a continuous flow path was observed over a wide range of gas-water ratios from 10^{-1} to 10^{4}. The width of the flow path increases as gas rate increases. This flow path, however, was continuously being broken up by the water phase and reforming again. Figure 3.3 illustrates some examples.

This flow mechanism shows the unsteady nature of the experiment. Even at constant gas and liquid injection rate, pressure fluctuates and saturation changes as fracture space change from being a gas path to water path and vice versa. This emphasizes the importance of acquiring instantaneous pressure, saturation and flow rate measurements.

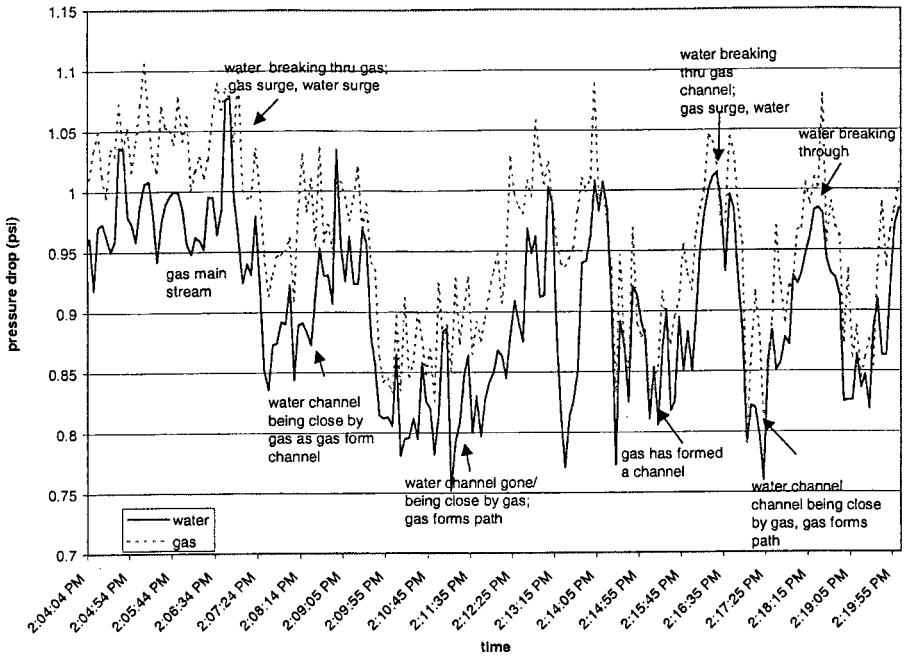

Figure 3.1 Pressure fluctuations cause by the breaking and reforming of gas flow path.

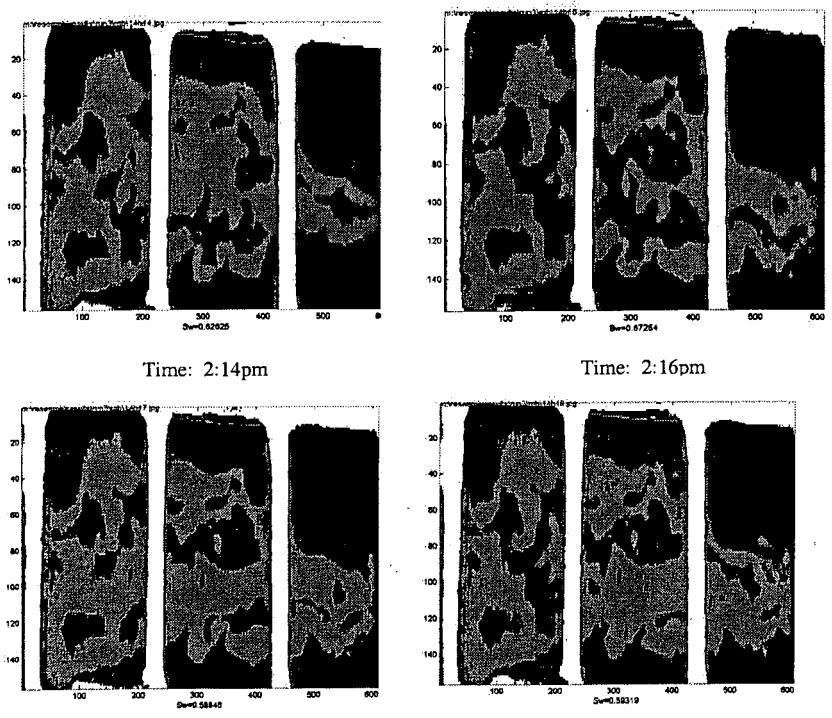

Time: 2:14pm

Time: 2:16pm

Time: 2:17pm

Time: 2:18pm

Figure 3.2 Images showing the forming and breaking of gas flow path corresponding to the time in Figure 3.1.

Gas rate: 0.5 cc/min water rate 8.5 cc/min

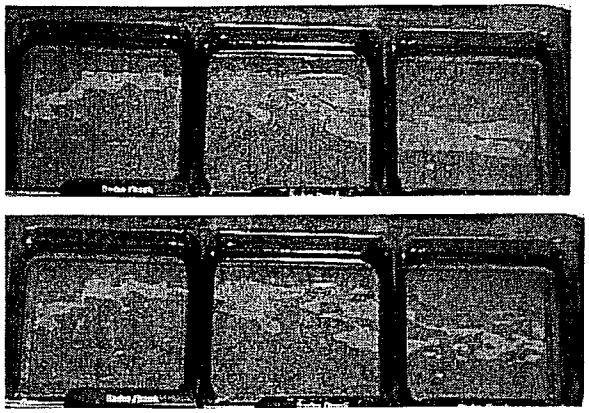

Gas rate: 19 cc/min water rate 8.5 cc/min

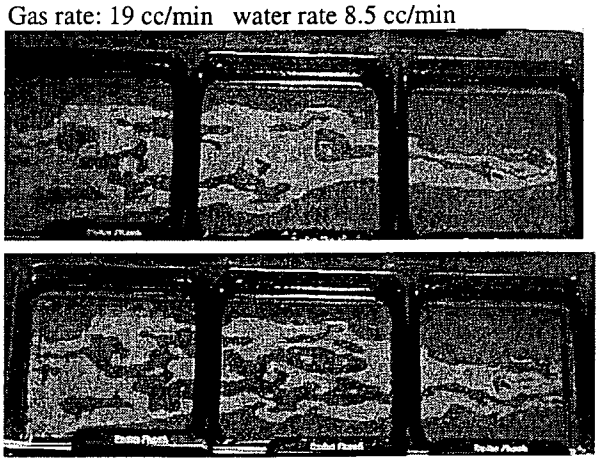

Gas rate: 140 cc/min water rate 8.5 cc/min

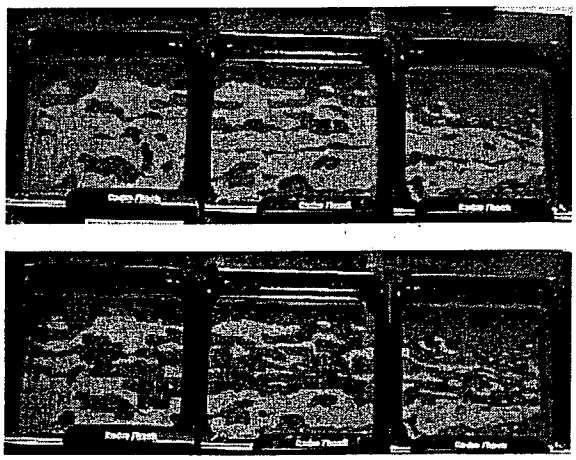

Figure 3.3 Examples of gas flow path increase in width as gas flow rate increases and water breaking up this flow path.

Persoff and Pruess (1995) observed a similar flow mechanism in their experiment with air-water flow in a transparent fracture replica. They also related the pressure fluctuations with the blocking and unblocking of flow path. They modeled the behavior as flow through a cylindrical tube of constant radius with a certain critical throat point of radius very much smaller than the tube. Through their model they were able to prove that a phase flow path in fractures will be unstable and will consequently be invaded by the other phase. This observation is also consistent with the findings by Su et al. (1999), Kneafsy and Pruess (1998) and numerical simulation by Pruess and Tsang (1990) where the flow mechanism was described as intermittent localized flow.

Intermittent localized flow observation is contrary to that of the concept of moving "islands" or flow structures carried by one phase as observed by Fourar and Bories (1995), Fourar et al. (1993), and Pan et al. (1996). The superficial velocities for the smooth-walled experiment are graphed on Fourar and Bories (1995) flow pattern map in Figure 3.4. Although, the data covered a wide range of the proposed flow patterns, these flow patterns were not seen in the experiment here. The intermittent localized flow observed is more comparable to flow in porous media. Phases in the experiment move only through continuous phase paths like in porous media. But unlike porous media, the phase paths or occupancy are not constant but are rapidly changing and reforming.

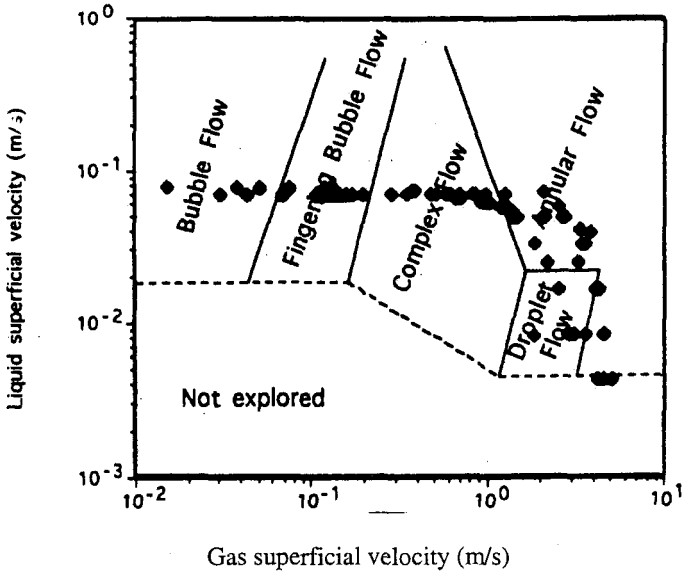

Figure 3.4 Smooth-walled fracture experimental velocity data imposed in Fourar and Bories (1995) flow map for glass channel.

3.1.2 Relative Permeability Curve From Porous Medium Approach

Eqn. (1.4) and Eqn. (1.5) for Darcy flow of two-phase flow were used to calculate relative permeabilities. The use of these equations requires the knowledge of the fracture

absolute permeability. The absolute permeability was derived using Eqn. (1.1) with the pressure drop and flow rate coming from single-phase liquid experiments.

Two single-phase experiments were done. The results of these are illustrated in Figure 3.5. Run #1 was done in sequence with the smooth-walled experiments. After noticing that the absolute permeability changes with flow rate Run #2 was done several weeks later with a different pump to investigate a wider flow rate range. Both runs show that for pressures bellow 0.5 psi, k_{abs} is changing with flow rate. This is implies that the fluid is lifting the glass as it flows through the fracture. At pressures greater than 0.5psi, the glass is lifted to its maximum height defined by the confinement of the metal frame. At this pressure range, the absolute permeability is constant. All the data points in the experiment lie in this range of constant absolute permeability (see Appendix B). However, the results of the two experiments were conflicting in terms of magnitude. The choice of which absolute permeability to use will affect the magnitude of the calculated relative permeability but will not affect the shape of the relative permeability curve. The highest absolute permeability derived from Run #1 was used.

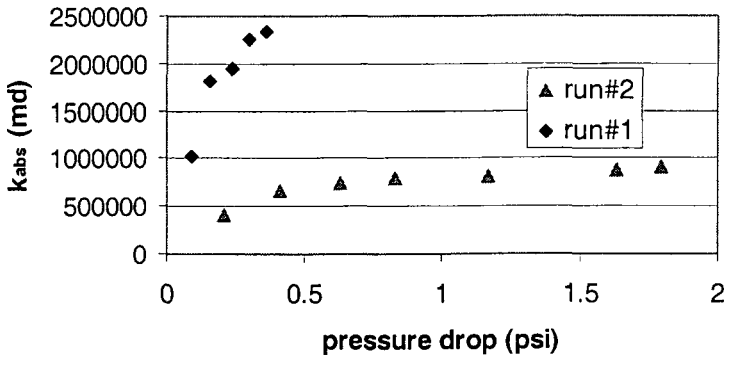

Figure 3.5 Absolute fracture permeability derived form single-phase liquid experiments for smooth-walled fracture

Appendix B shows the detailed calculation of relative permeability. The results are graphed in Figure 3.6. In this figure, neglecting the data enclosed in blue square box, the relative permeability curve has the shape of Corey curve (Corey, 1954). This follows with the observation that the flow in the smooth-walled fracture is comparable to flow in porous media. It is also noticeable that the sum of the relative permeabilities at a particular saturation is less than unity. This indicates phase interference. This is consistent with the observed flow mechanism where the gas and water compete in establishing pathways through the fracture.

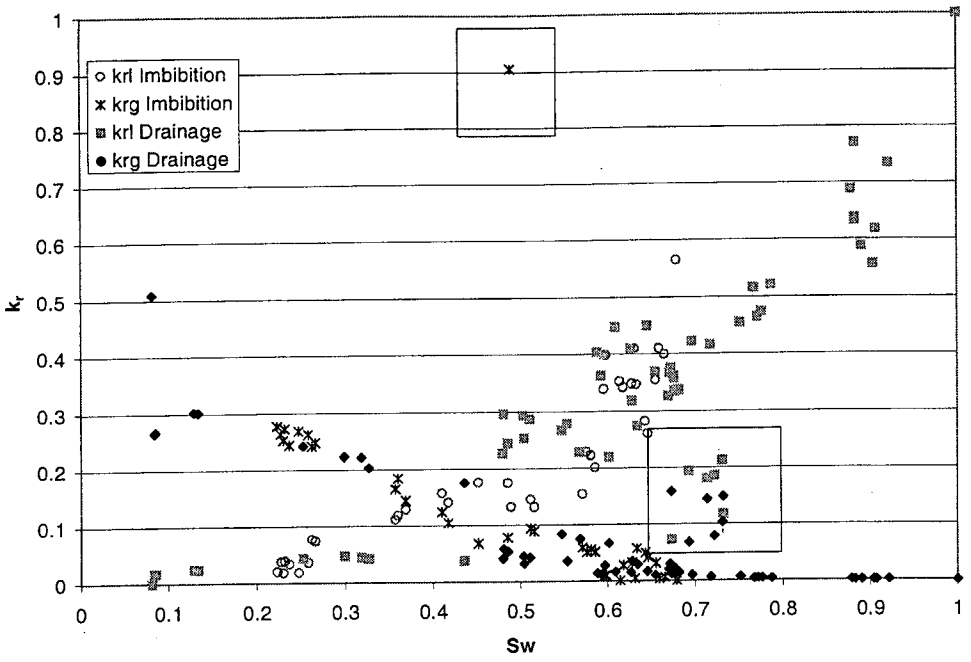

Figure 3.6 Relative permeability data obtained from smooth-walled fracture experiment

The data for both imbibition and drainage experiments were fitted separately with the Honarpour et al. (1982) expression:

$$k_{rw} = k_{rwo}\left[\frac{(S_w - S_{wr})}{(1 - S_{wr} - S_{gr})}\right]^{n_w} \tag{3.1}$$

$$k_{rg} = k_{rgo}\left[\frac{(1 - S_w - S_{gr})}{(1 - S_{wr} - S_{gr})}\right]^{n_g} \tag{3.2}$$

with

$$k_{rwo} = k_{rw}(S_{wi}) \tag{3.3}$$

$$k_{rgo} = k_{rg}(S_{wr}) \tag{3.4}$$

S_{wi} being the initial water saturation for drainage while for imbibition

$$k_{rwo} = k_{rw}(S_{gr}) \tag{3.5}$$

$$k_{rgo} = k_{rg}(S_{wi}) \tag{3.6}$$

The resulting curves are graphed in Figure 3.7 and Figure 3.8. The parameters for the fitted curved are tallied in Table 1. In both graphs, the fitted Honarpour curves give good representation of the trend of relative permeability data with saturation. The fitted curves have different exponents for the Honarpour expression for imbibition and drainage. This is even though the data for both drainage and imbibition seem to lie in same trend as seen in Figure 3.6. This shows the effect of saturation history on relative permeability. Compared to the Corey expression from Eqn. (1.9) and (1.10), the drainage experiments have dissimilar exponents. For imbibition, however, the value of n_w (4.57) and n_g (1.92) are close to Corey exponents of 4 for n_w and 2 for n_g.

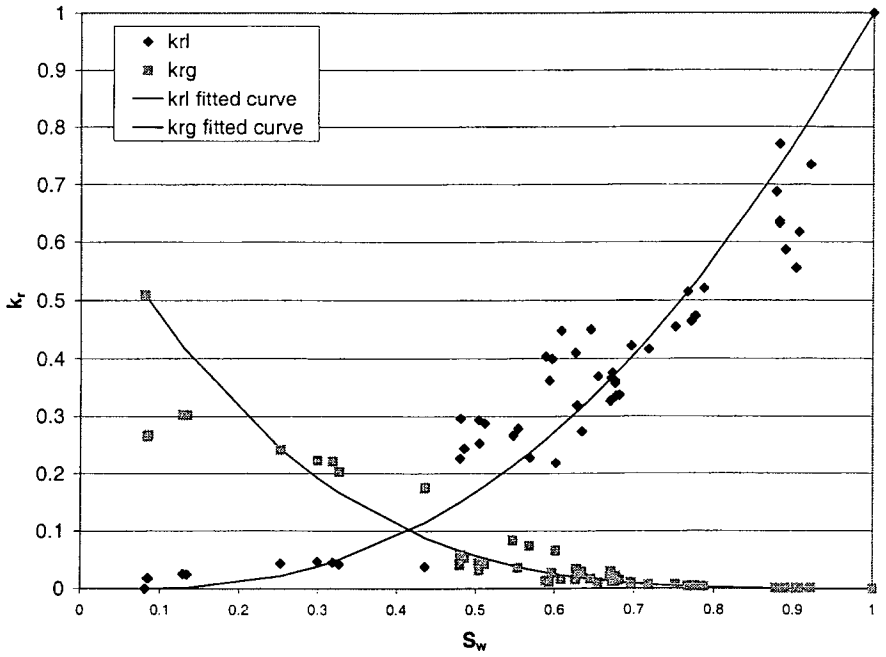

Figure 3.7 Fitted Honarpour expression for smooth-walled fracture drainage experiment.

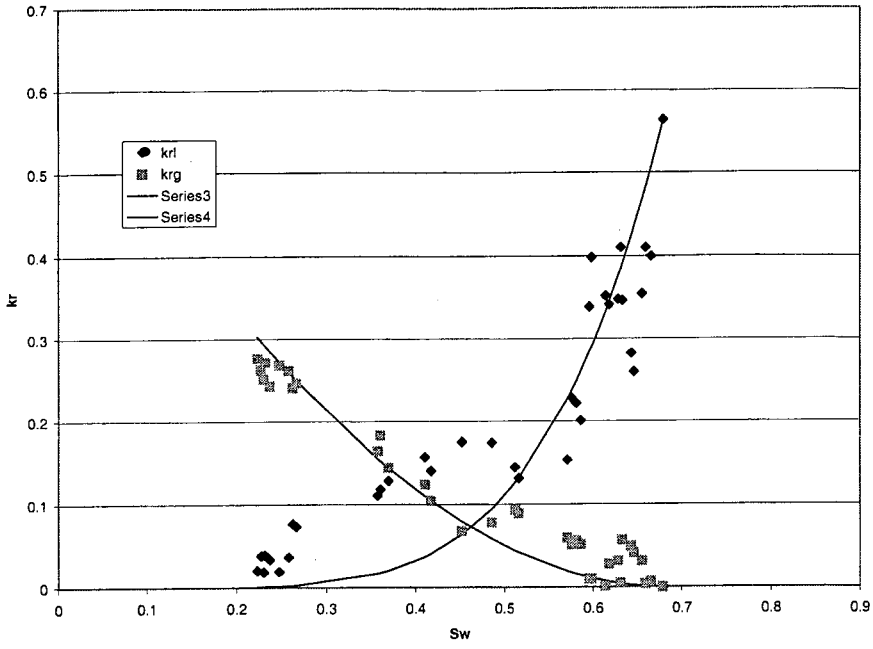

Figure 3.8 Fitted Honarpour expression for smooth-walled fracture imbibition experiment.

Table 1 Fit Parameters for smooth-walled fracture experiment

	Drainage	Imbibition
Swr	0.081	0.081
Sgr	0	0.321
krwo	1	0.564
krgo	0.509	0.509
nw	2.27	4.57
ng	3.59	1.92

3.1.3 Application of Homogenuous Single-Phase Pipe Flow Model for Smooth-walled Fracture

The homogeneous single-phase pipe flow model was also applied in the data for the smooth-walled fracture. The table of calculation for this model is included in Appendix B. Figure 3.9 depicts the calculated friction factor with the modified Reynold's number in a log-log chart. From the fitted linear equation, the constants C and n in Eqn. (1.17) are 3.23 and 0.75 respectively. Figure 3.10 compares this result to previous works for parallel plate experiments. The slope of the fitted line (-0.75) is lower than the usual finding of negative unit slope for laminar flow. Among all the studies, the data is closer to Romm (1966).

The fit of Eqn. (1.17) for friction factor as a function of Reynold's number with the experimental data is not so good. Thus, pressure drop calculated from Eqn. (1.12) inadequately predicts the experimental data (see Figure 3.11). This was expected since the observed flow mechanism was not similar to flow regimes in pipes on which this model is based.

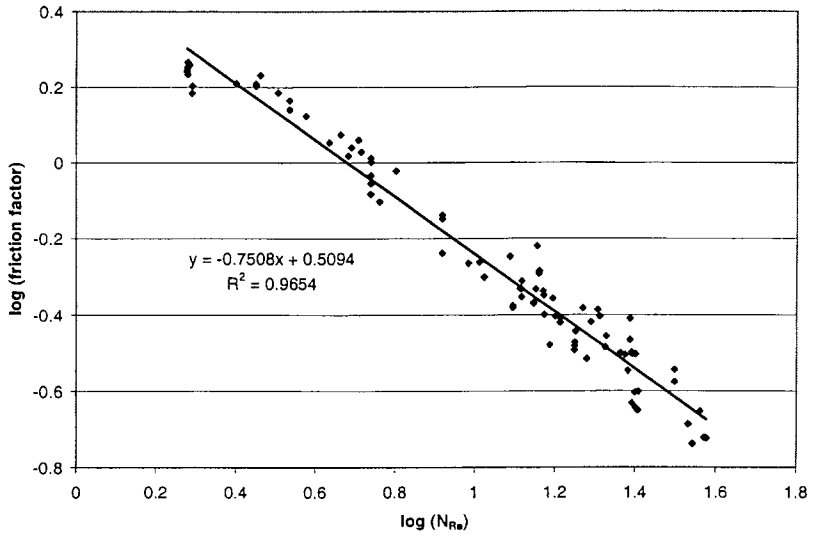

Figure 3.9 Natural logarithm of friction factor with natural logarithm of Reynold's number from data of smooth-walled fracture experiment.

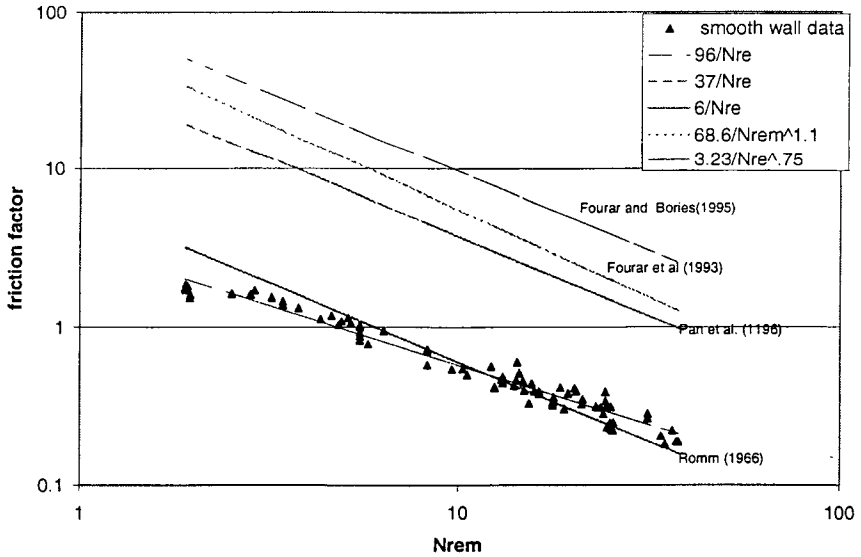

Figure 3.10 Friction factor against modified Reynold's number for smooth-walled fracture in comparison to previous works.

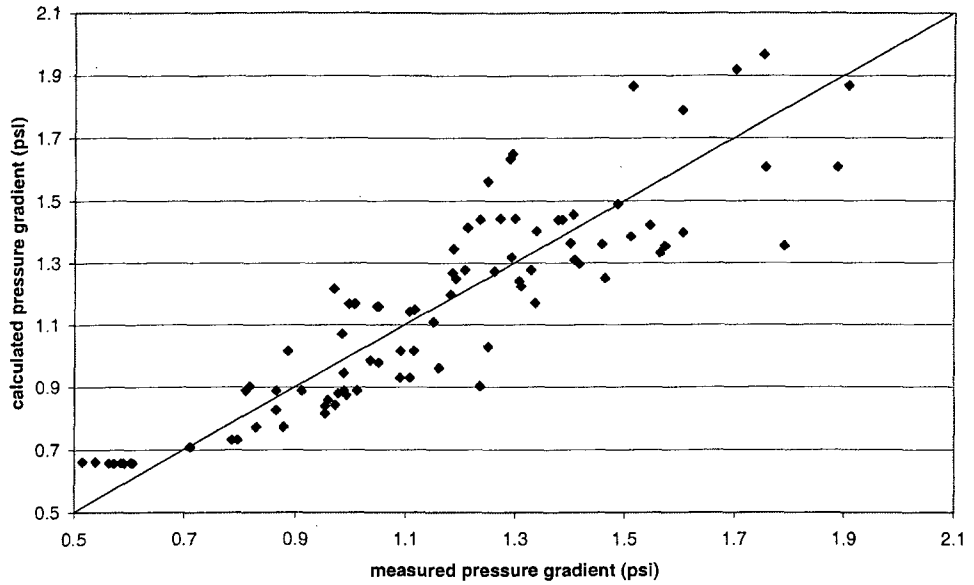

Figure 3.11 Comparison of the predicted pressure drop from homogeneous model and measured data for smooth-walled fracture.

3.2 Rough-walled Fracture Experiments

3.2.1 Observed Flow Mechanism

Similar to the smooth-walled fracture experiments, a phase in the rough-walled fracture experiment during drainage moved by establishing a continuous flow path for itself. However, the stability of the phase path varied greatly with gas-water ratio.

At low gas-water ratio, the gas invades the liquid-dominated fracture and establishes a path (see Figure 3.12). The path built is wider than that in the smooth-walled fracture at the same gas-water ratio. This maybe because the mesh gives the gas a way to move horizontally in the fracture even at low gas-water ratio. This path is very unstable. Water quickly invades it almost completely leaving few scattered residual gas areas. The residual gas areas left are not enough to establish a path. Thus, the fracture after the invasion of water can be said to return to its liquid-dominated condition. Within this liquid-dominated condition, the gas will again construct its own flow path and the cycle continues. Figure 3.13 shows two examples of gas flow channels, the water invasion that proceeds it and the residual gas areas left after the water invasion.

The formation of the gas path and the consequent water invasion again goes along with pressure fluctuations. Figure 3.14 shows the pressure data for Figure 3.12 and picture set (A) in Figure 3.13. Similar to the smooth-walled fracture (see Section 3.1.1), the low pressure drop corresponds to the forming of the gas path, followed by a peak of both gas and liquid pressure related to the surge of the two fluids through the fracture. It was

observed that the magnitude of the pressure peaks decreases as the gas-water ratio increases.

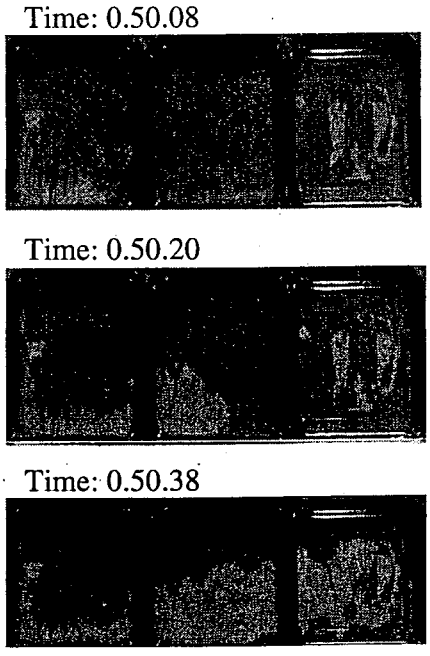

Figure 3.12 Gas invasion in drainage experiment with rough-walled fracture.

The diminishing magnitude of the pressure fluctuations relates to the point when the gas has established a stable path. With a stable path, gas can travel more smoothly and surge flow does not occur. Without surge flow, large pressure fluctuations are not observed. A stable gas path was reached at high gas-water ratio. As in the smooth-walled fracture, the stable gas channels increase in width with increasing gas-water ratio (see Figure 3.15). Within these established gas paths, water sometimes forms narrow channels but these channels are unstable. Water flow is mostly at the edge of the gas path. In the ratios of stable phase paths, saturation can be considered constant at one gas-water injection rate.

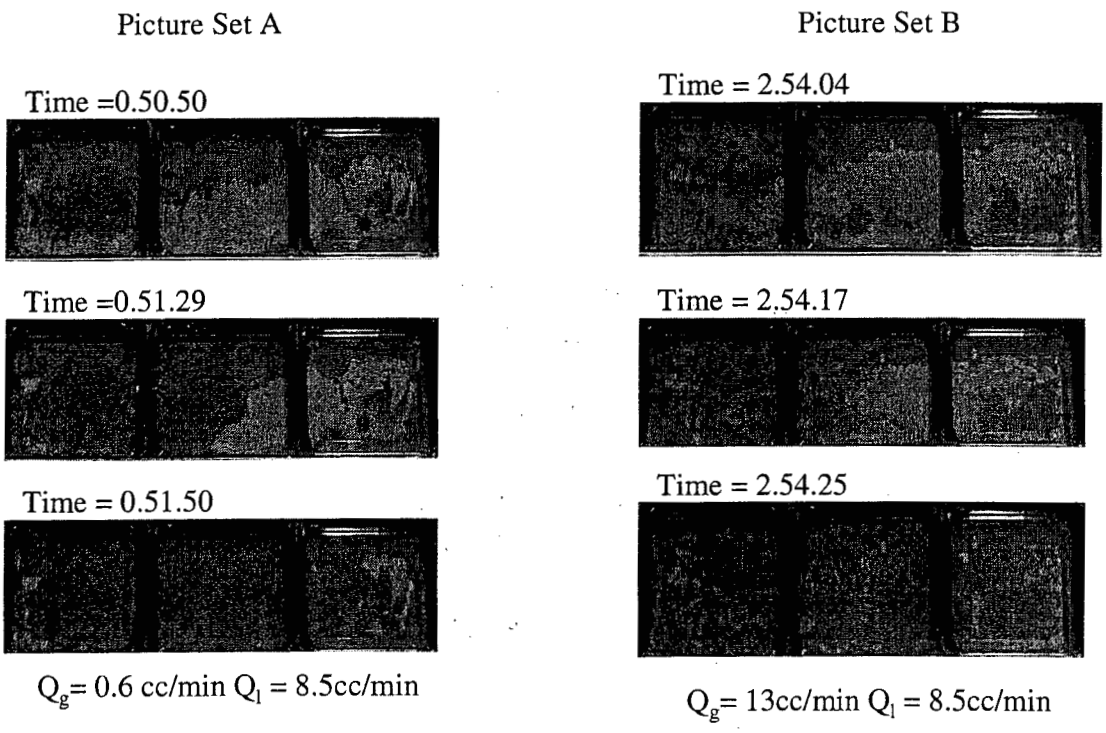

Figure 3.13 Examples of gas flow path, the invasion of water that follows and the residual gases left in rough-walled drainage experiment.

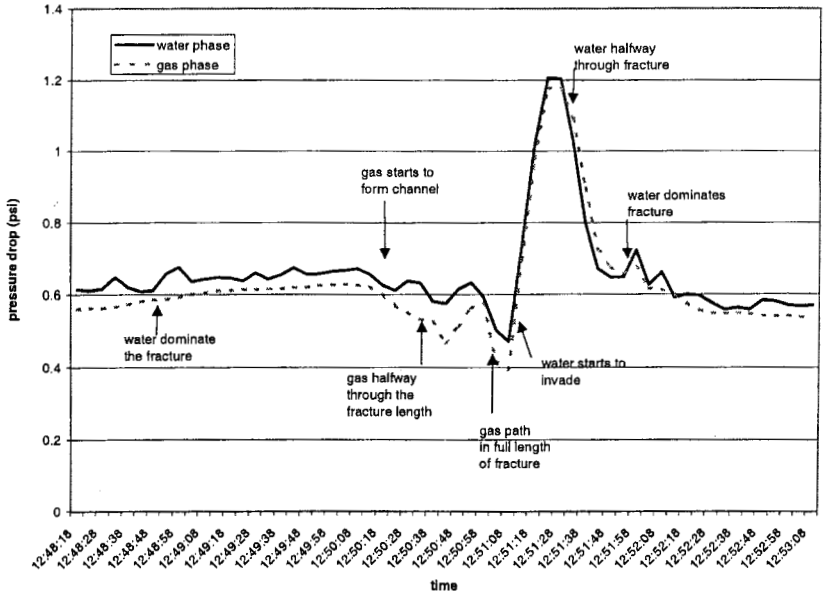

Figure 3.14 Example of pressure fluctuations caused by the building and breaking up of gas and water path. Pictures for this time span is shown in Figure 3.12 and picture set A in Figure 3.13.

For the imbibition experiment, two flow mechanisms were observed. At low gas-water ratio, a stable flow path was seen (see Figure 3.16). This stable flow path is similar to that in the smooth-walled fracture and for the drainage experiment in the rough-walled fracture. At high gas-water ratio (50 and above), a wave-like flow similar to flow in pipe was observed. In this flow, water travels like wave or a steady front covering the entire fracture. This wave flow caused an increase in the pressure drop exceeding the maximum of the pressure transducer. Thus, the magnitude of the pressure drop when a wave front occurs can be higher than 5psi. Figure 3.17 shows a sample of wave-like front and its corresponding pressure peaks.

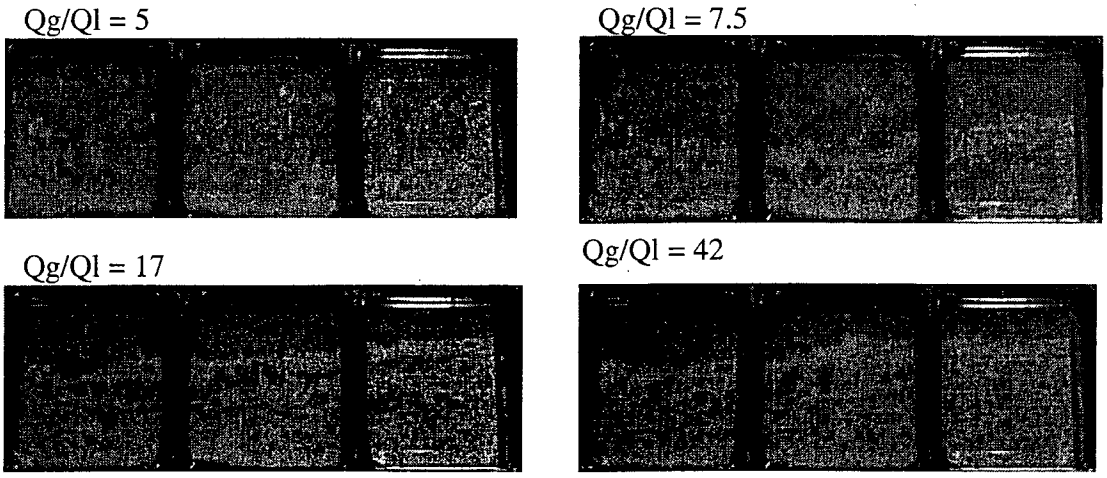

Figure 3.15 Images showing stable gas path in high gas-water ratio for rough-walled fracture.

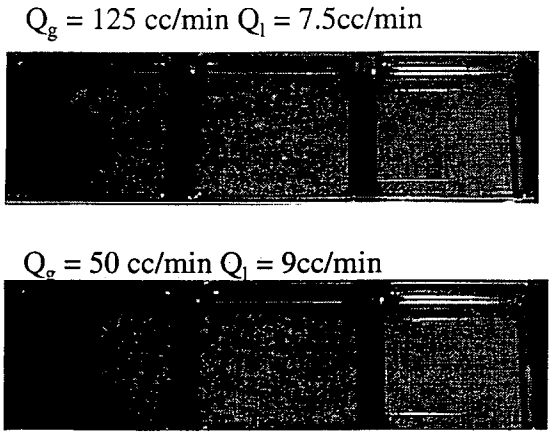

Figure 3.16 Images showing examples of stable flow path of imbibition experiment in the rough-walled fracture.

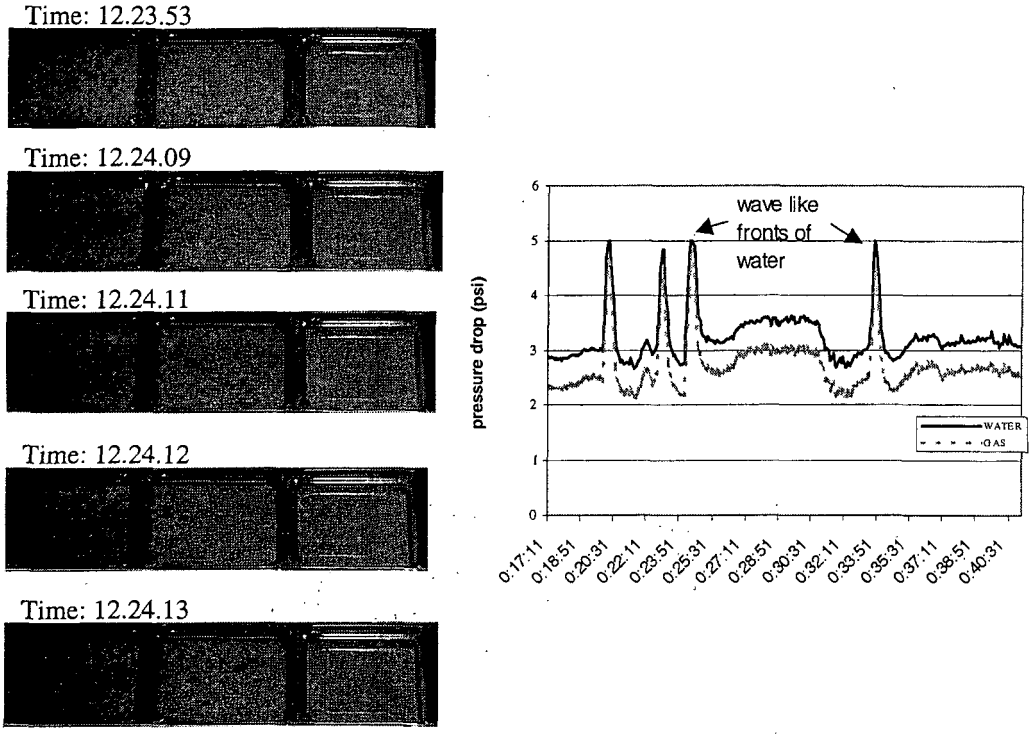

Figure 3.17 Picture of wave-like fronts seen in high gas-water ratio at imbibition experiment and its corresponding pressure peaks.

In all the experiments for the rough-walled fracture, there was considerable amount of trapped phases in the fracture as seen in the red and white isolated spots in pictures from Figure 3.12 to Figure 3.17. This is likely since the mesh provided small corners for the wetting phase to cling to and be trapped in the gas-dominated area of the fracture. It also provided a means to trap the nonwetting gas phase in the small empty space of the mesh as the water surrounds the walls.

3.2.2 Relative Permeability Curve Through Porous Medium Approach

The calculation procedure done in Section 3.1.2 for relative permeability was repeated for the data gathered in the rough-walled fracture experiments. A detailed list of the values is shown in Appendix B.

Several single-phase rough wall experiments were done to determine the absolute permeability of the fracture. The calculated absolute permeabilities from these experiments are shown in

Figure 3.18. The reason for the variation of the absolute permeability value with pressure was discussed in Section 3.1.2. As in the smooth-walled fracture, the absolute permeability remains constant at pressures greater than 0.5 psi. Since all the experiments

were at pressures higher than 0.5 psi, absolute permeability was taken as the average of the measurements with pressures greater than 0.5 psi. The absolute permeability value used was 1,950 darcy.

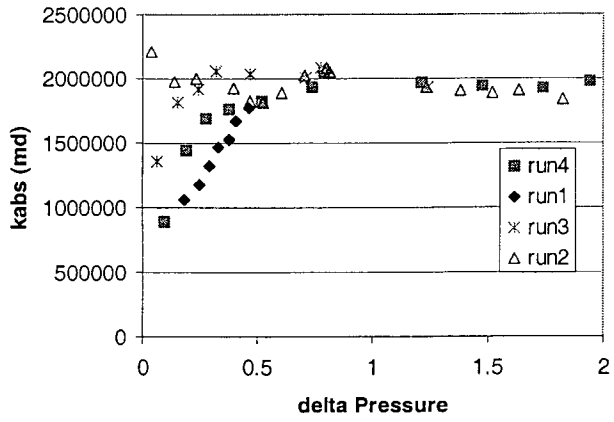

Figure 3.18 Absolute permeability from single-phase experiments for rough-walled fracture model.

Figure 3.19 shows the complete data from the drainage experiment for the rough-walled apparatus. This graph shows the relative permeability taken when the gas path was an unstable surging conduit and when it was a stable channel. Noticing that the flow is more comparable to porous flow when the gas has established a stable path, the data for the unstable gas surge was removed. The remaining data are seen in Figure 3.20. This figure displays a more defined trend. This indicates that the porous medium approach is more applicable to model flow through the rough-walled fracture when flow is characterized by established phase paths. It also suggests that other means of data analysis is needed for the data corresponding to unstable gas surge.

For imbibition, the calculated relative permeability for all types of flow mechanism observed is seen in Figure 3.21. The graph of relative permeability is too scattered showing no obvious relationship. One factor that may have caused this is the uncertainty with regards to saturation measurement for the imbibition experiment of rough-walled fracture. The picture for the imbibition experiment has lower picture quality than the other experiments and saturation analysis was more difficult due to trapped water and gas phase scattered throughout the flow area. Figure 3.22 demonstrate how the programs for saturation measurement were unable to capture the finer details of trapped phases. This effect diminishes as the stable fluid pathway is established with decreasing gas-water ratio.

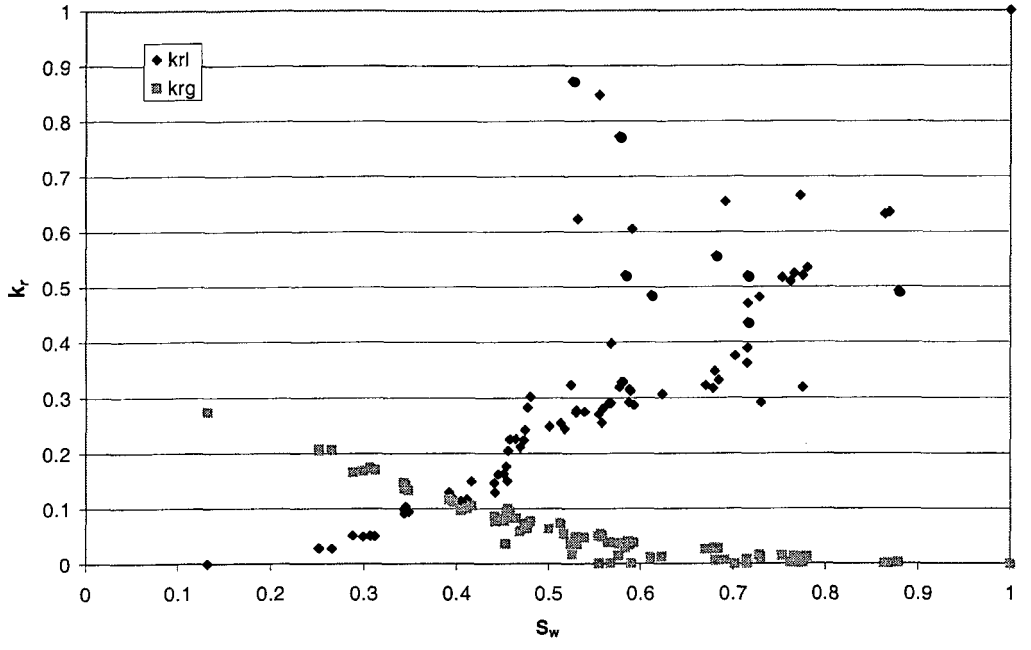

Figure 3.19 Relative permeability data for drainage experiment for rough-walled fracture model.

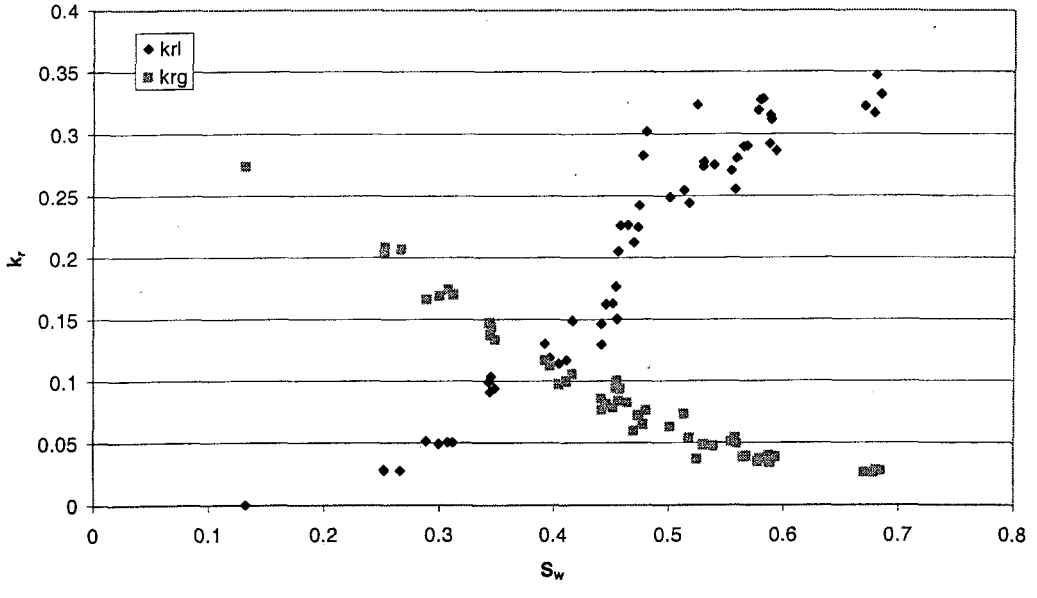

Figure 3.20 Relative permeability data for rough-walled model when the gas path is stable.

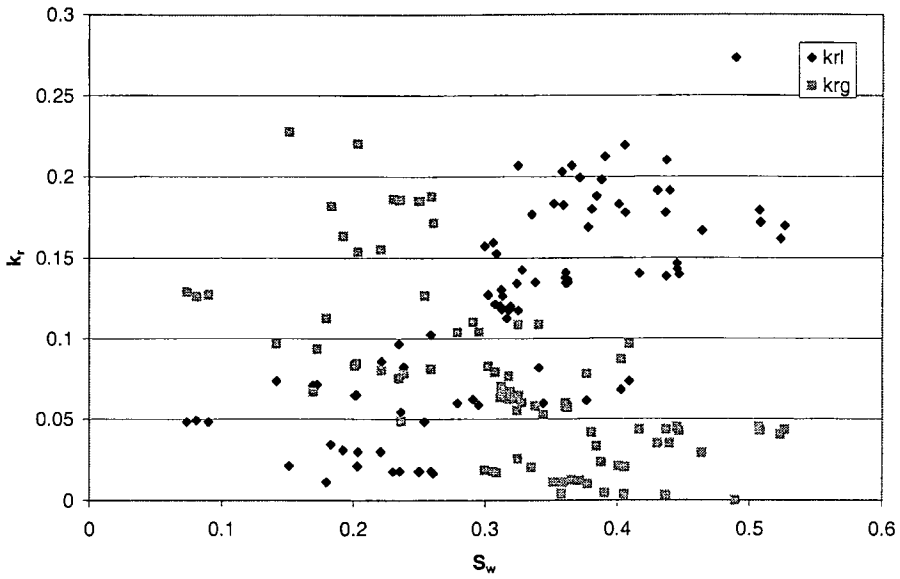

Figure 3.21 Relative permeability data for rough-walled fracture imbibition experiment.

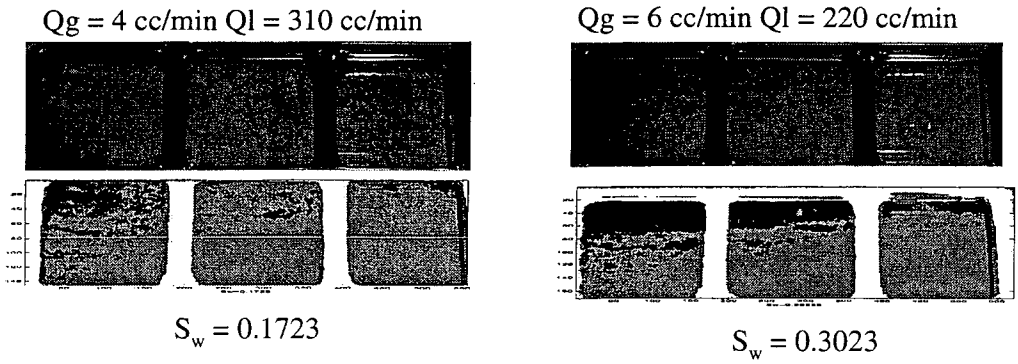

Figure 3.22 Examples of saturation measurement for imbibition experiment with rough-walled fracture.

The data corresponding only to flow characterized by stable fluid pathway was chosen and graphed in Figure 3.23. Although Figure 3.23 is an improvement over Figure 3.21, the association between relative permeability and saturation is still unclear. These data for imbibition are graphed along with the drainage data in Figure 3.24. This graph shows that relative permeability for the nonwetting phase in imbibition is lower than that of drainage while the opposite is true for the wetting phase. This is consistent with studies for oil-water systems (Amyx et al., 1960) and steam-water systems (Li et al., 1999). Amyx et al. (1960) noted that the imbibition process causes the nonwetting phase (oil) to lose its mobility at high values of wetting phase saturation while the drainage process causes the wetting phase to lose its mobility at higher values of wetting phase saturation.

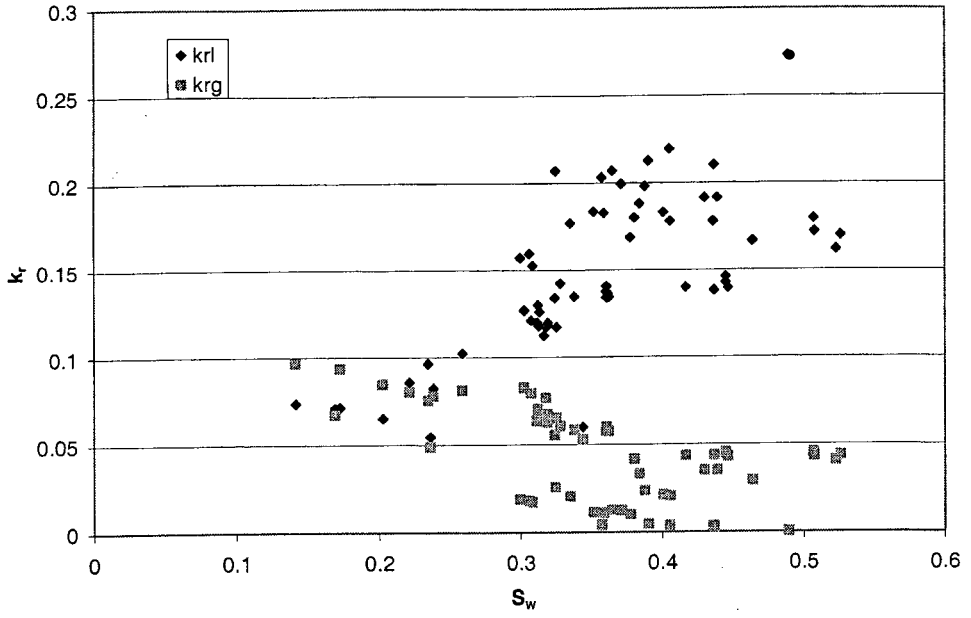

Figure 3.23 Relative permeability for rough-walled imbibition experiment for flow with stable phase path.

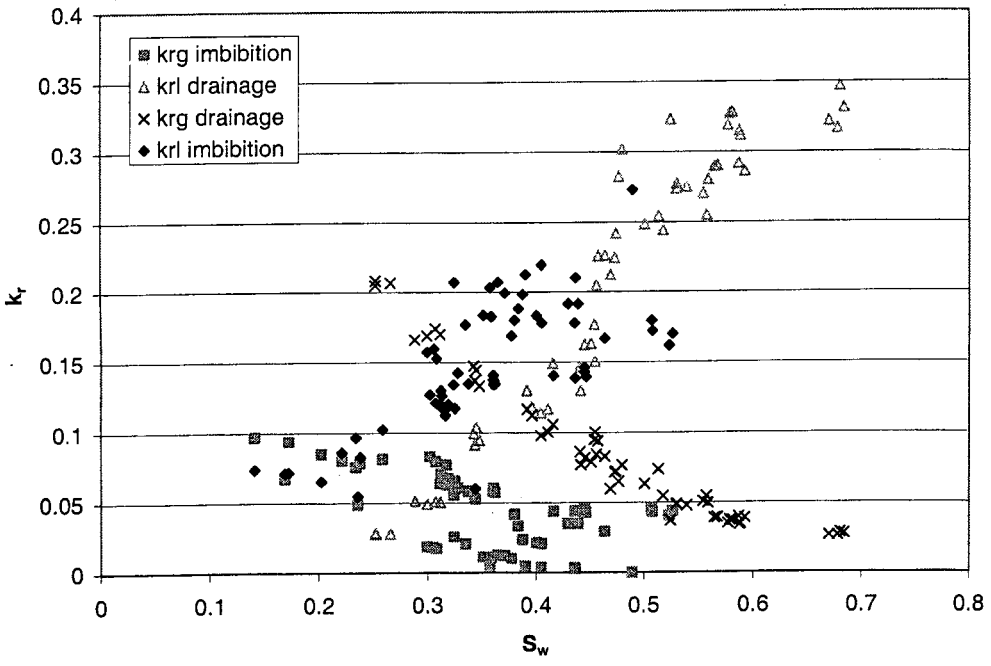

Figure 3.24 Drainage and imbibition data for rough-walled fracture.

The Honarpour relation in Eqn. (3.1) and Eqn. (3.2) was fitted to the drainage and imbibition data separately. The resulting fit parameters are tabulated in Table 2. As expected, there is a good fit with the drainage data but not with the imbibition data. The exponents of the fitted curves are different for imbibition and drainage and both are far from Corey values.

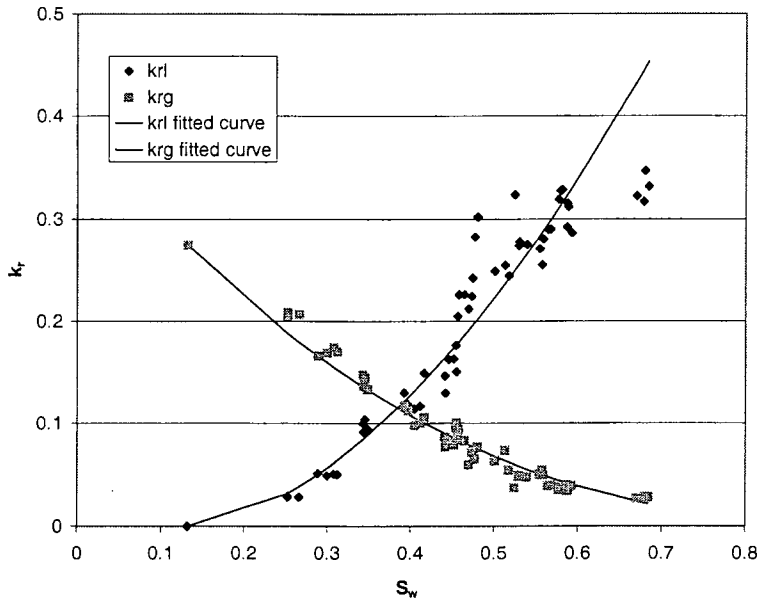

Figure 3.25 Fitted Honarpour curve for drainage data in rough-walled fracture experiment.

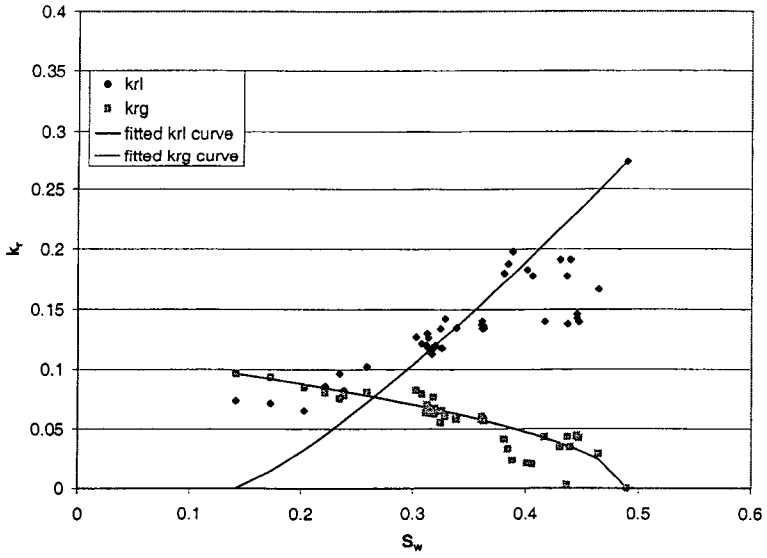

Figure 3.26 Fitted curve for imbibition rough-walled fracture experiment.

Table 2 Honarpour fit parameters for rough-walled experiment.

	Drainage	Imbibition
Swr	0.132	0.141
Sgr	0	0.51
krwo	1	0.27
krgo	0.274	0.1
nw	1.75	1.2
ng	2.53	0.52

3.2.3 Application of Homogeneous Model for Rough-Walled Fracture Experiment

It was discovered in the previous section that the porous medium approach when applied only through flow characterized by stable phase paths yields better defined relative permeability curves. This indicates that different flow mechanisms may require different mathematical approaches. Thus in the application of the homogeneous model to the rough-walled fracture experiment, the appropriateness of the model was reviewed for all data and for data corresponding only to unstable surge flow.

The natural logarithm of the calculated friction factor and Reynold's number is seen in Figure 3.27. Graph A includes all the data while graph B consists only of the data corresponding to unstable surge flow. Comparisons of graphs A and B shows that removing the stable flow data removed the cluster of data points. The observation that stable flow data tend to cluster in plots of friction factor with Reynold's number suggests that the homogeneous single-phase model is not the appropriate model for this kind of flow. However, considering only the surge data as was done in graph B of Figure 3.27 also did not improve the goodness of fit. For both graphs, there exist some data points that lie vertically with respect to each other. This can indicate either two things that the friction factor may not be a sole function of Reynold's number or that Reynold's number is not a good correlation variable for friction factor in flow through fractures. The calculated friction factor and Reynold's number are compared to other data in Figure 3.28. Again both data sets have slopes lower than unity and the data are closer to Romm's expression (Romm, 1966). The values for the constants C and n are listed in Table 3. The pressure drop calculated from these values are compared to measured data in Figure 3.29. Since the fit of the friction factor with the experimental data was not so good, the computed pressure drop from Eqn. (1.12) was not able to satisfactorily predict the experimental pressure gradient.

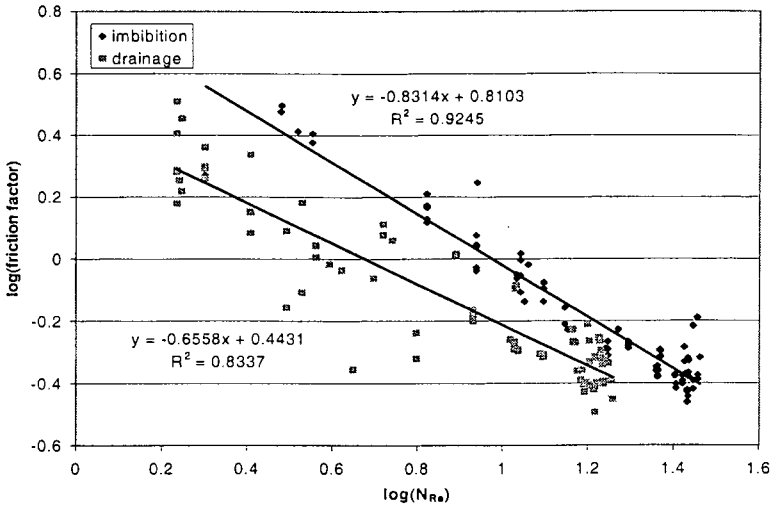

(A)

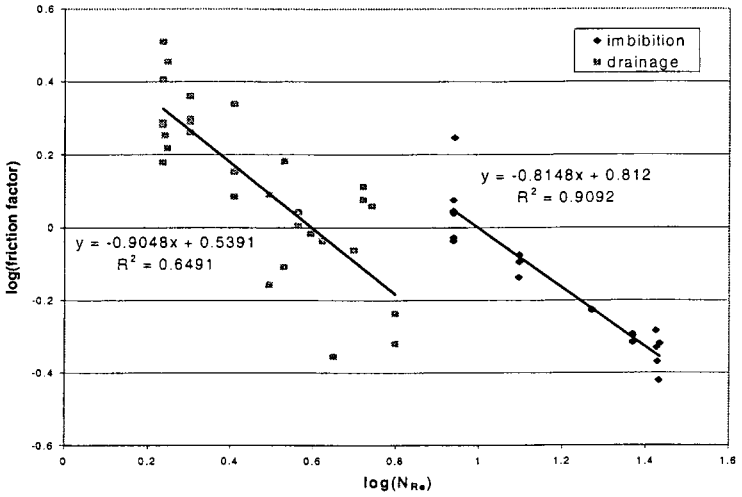

(B)

Figure 3.27 Natural logarithm of friction factor with natural logarithm of Reynold's number for (a) all rough-walled data and (b) for data with unstable surge flow.

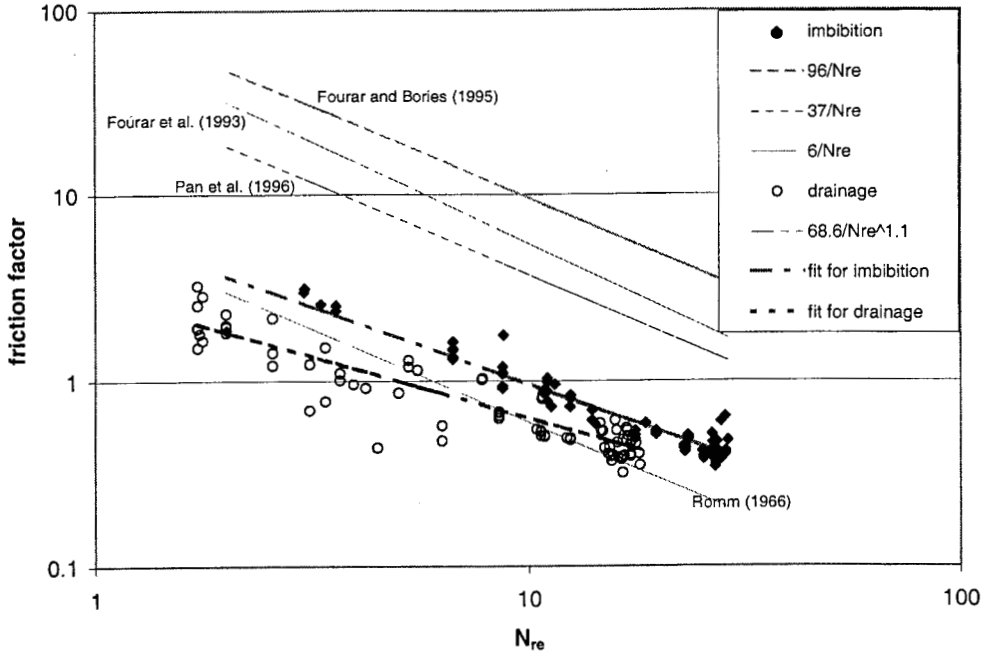

Figure 3.28 Friction factor with modified Reynold's number for rough-walled experiment.

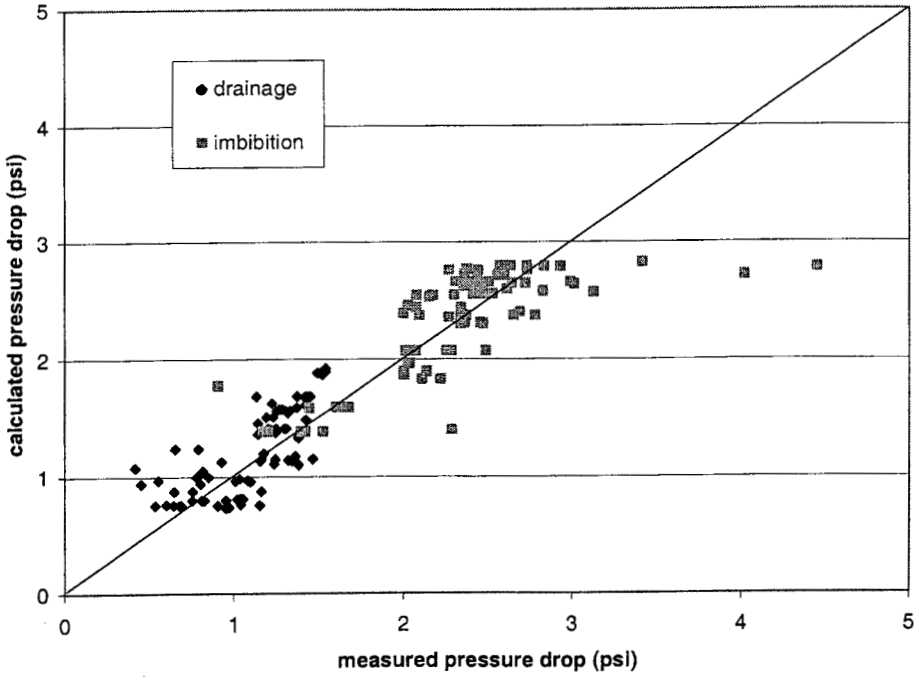

Figure 3.29 Comparison of the measured pressure drop against calculated pressure drop from homogeneous equivalent single-phase model.

Table 3 Homogeneous equivalent single-phase fit parameters.

Experiment	C	n
Imbibition rough wall experiment	6.5	-0.83
Drainage for rough wall experiment	2.8	-0.66
Smooth wall experiment	3.23	-0.75

3.3 Comparison of Smooth- and Rough-Walled Experiment to Other Studies

The data for both smooth and rough-walled experiments were entered in Figure 1.1 for comparison to previous studies and to known correlations for porous media (see Figure 3.30). Compared to other data, the experimental data in this study is higher than that of Persoff and Pruess (1995) experiments but lower than Persoff (1991). With this, no apparent conclusion can be made as to whether the data from this study contradicts or agree with previous relative permeability experiments. However, more importantly Figure 3.30 shows that the experimental data mostly conform to Corey type of relative permeability curve. This suggests that flow through fractures can be analyzed by treating it as limiting case of porous media and by using the relative permeability variable. The relative permeabilities as seen in Figure 3.30 for fractures sum up to less than one and are not in linear relationsip with saturation as suggested by the X-curve. This reiterates results from previous studies that phase interference in fractures does occur. Comparing the results for smooth and rough fractures, the relative permeability values for the smooth and the rough-walled drainage experiment do not differ much. However, the relative permeability for imbibition experiment in the rough-walled fracture is lower than these two experiments.

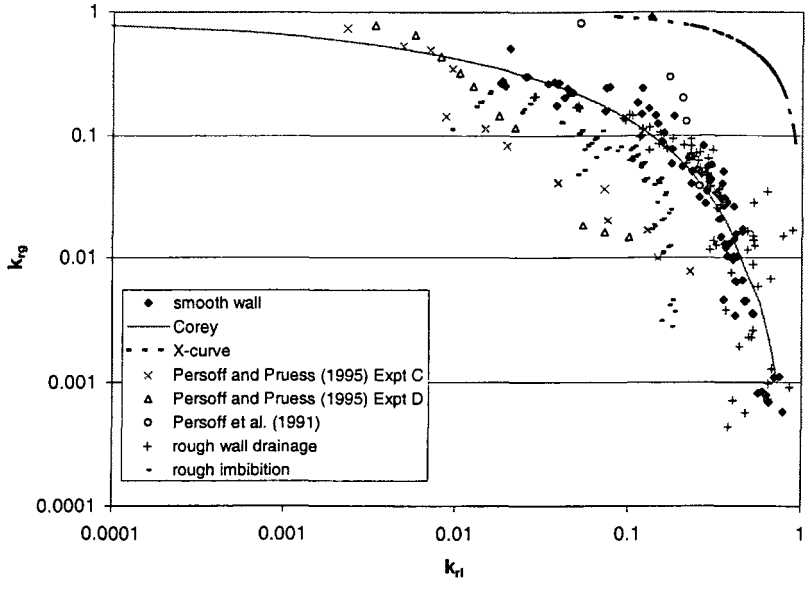

Figure 3.30 Comparison of relative permeability data with previous work on rough-walled fractures.

Chapter 4

4 Conclusions and Recommendations

The experiments and analysis presented in this paper have led to the following conclusions:

1. Two-phase flow through smooth and rough parallel plate fractures is characterized by each phase establishing localized continuous flow paths. The stability of these flow paths is dependent on the flow rate ratio of the phases. A phase flow path undergoes constant cycles of breakage and reformation as certain points are blocked and unblocked by the other phase. The breaking and reforming of phase paths cause pressure, flow rate and saturation fluctuations even at constant input conditions. This reveals the unsteady nature of flow through fractures.

2. The imbibition process through a rough-walled fracture also undergoes wave-like flow similar to flow in pipes at high gas-water ratio. Other than this, flow through smooth- and rough-walled fractures is more similar to flow in porous media where a phase moves by establishing continuous channels. The flow mechanism of having moving discontinuous flow structures as bubbles or "islands" carried along by another continuous phase was not observed throughout the experiments.

3. Two-phase flow through smooth- and rough-walled fractures can be modeled adequately by a porous medium approach. In this approach, Darcy's law governs flow and phase interference is represented by the relative permeability variable. The resulting relative permeability curve from experimental data shows a clear relationship between relative permeability and phase saturation. The experimental relative permeability curves follow the Corey shape and can be fitted to reasonable accuracy by the Honarpour expression.

4. There is considerable phase interference in flow through fractures. This is deduced from the sum of the gas and liquid relative permeability for all experiments being less than unity.

5. The equivalent homogenous single-phase approach did not give satisfactory representation of flow through fractures. The graphs of experimentally derived friction factor with the modified Reynold's number do not reveal distinctive linear relationship. This leads to inadequate pressure drop prediction of the model.

The apparatus and methodology used in this study proved to be an effective means of investigating flow through fractures. However, improvement is needed to ensure control

of fracture aperture i.e. preventing the glass plate from being lifted by the flowing fluids. The method for saturation measurement is dependable when picture quality is good and when distinct boundaries of phases are seen. It is recommended to experiment with techniques for enhancing picture color contrasts. This will improve the program's accuracy in differentiating phases. This will be useful for cases when small isolated phases are dispersed throughout such as the case in imbibition for rough-walled fractures.

It is recommended that further experiments with smooth-walled fractures be done this time with certainty as to the fracture absolute permeability. This is to establish the magnitude of relative permeability in smooth-walled fractures. It is also recommended to conduct experiments to investigate other variables in fracture flow that were not included in this study such as effect of aperture, viscosity, gravity, degree of roughness etc.

Nomenclature

A = area
b = fracture aperture
C = constant in Blasium equation
f = friction factor
k_{abs} = absolute permeability
k_r = relative permeability
L = fracture length
n = constant in Blasium equation
N_{Re} = modified Reynold's number
p = pressure
Q = volumetric flow rate
q_l = Darcy flow velocity
S = saturation
V = superficial velocity
w = fracture width
Π = fracture perimeter
μ = viscosity
ρ = density

Subscripts:
g = gas phase
i = inlet
l = liquid phase
m = mean
o = outlet
r = residual
w = water

References

Amyx, J. W., Bass, D.M, and Whiting, R.L. *Petroleum Reservoir Engineering Physical Properties*, McGraw-Hill Book Co.,New York, 1960, pp 199-200.

Corey, A.T.,: The interrelationship between gas and oil relative permeabilities, *Prod. Mon.*, Vol. 19, 1954, pp. 38-41.

Fourar, M. and Bories, S.,: "Experimental Study of Air-Water Two-Phase Flow Through A Fracture (Narrow Channel)," *Int. J. Multiphase Flow* Vol. 21, No. 4, Toulouse, France (1995) pp. 621-637.

Fourar, M., Bories., Lenormand, R., and Persoff, P.,: "Two-Phase Flow in Smooth and Rough Fractures: Measurement and Correlation by Porous-Medium and Pipe Flow Models," *Water Resources Research* Vol. 29 No. 11. November 1993, pp. 3699-3708.

Hanselman, D. and Littlefield, B.: *Mastering Matlab 5 A Comprehensive Tutorial and Reference*, Prentice-Hall, Inc.,New Jersey, 1998.

Horne, R.H., Satik, C., Mahiya, G., Li, K., Ambusso, W., Tovar, R., Wang, C., and Nassori, H.: "Steam-Water Relative Permeability," *Proceedings of the World Geothermal Congress 2000*, Kyushu-Tohoku, Japan, May 28-June 10, 2000.

Kneafsy, T. J. and Pruess, K.,: "Laboratory Experiments on Heat-Driven Two-Phase Flows in Natural and Artificial Rock Fractures," *Water Resources Research* Vol. 34, No. 12, December 1998, pp. 3349-3367.

Li, K. and Horne, R.N.: "Accurate Measurement of Steam Flow Properties," *Proceedings of Geothermal Resource Council*, Reno, California, USA, October 17-20, 1999.

Lockhart, R. W. and Martinelli, R.C.,: "Proposed Correction of Data for Isothermal two-phase component flow in pipes," *Chem. Eng. Prog.*, Vol. 45, No. 39, 1949.

Pan, X., Wong, R.C., and Maini, B.B.: Steady State Two-Phase Flow in a Smooth Parallel Fracture, presented at the 47th Annual Technical Meeting of the Petroleum Society in Calgary, Alberta, Canada, June 10-12, 1996.

Persoff, P. K., Pruess, K. and Myer, L.: "Two-Phase Flow Visualization and Relative Permeability Measurement in Transparent Replicas of Rough-Walled Rock Fractures," *Proceedings 16th Workshop on Geothermal Reservoir Engineering*, Stanford University, Stanford, California, January 23-25, 1991.

Persoff, P., and Pruess, K.: "Two-Phase Flow Visualization and Relative Permeability Measurement in Natural Rough-Walled Rock Fractures," *Water Resources Research* Vol. 31, No. 5, May, 1995, pp. 1175-1186.

Pruess, K., and Tsang, Y. W.: "On Two-Phase Relative Permeability and Capillary Pressure of Rough-Walled Rock Fractures," *Water Resources Research Vol.* 26 No. 9, September 1990, pp 1915-1926.

Scheidegger, A.E. *The Physics of Flow Through Porous Media*, 3rd ed., University of Toronto, Toronto. 1974.

Su, G. W., Geller, J. T., Pruess, K. and Wen, F.,: " Experimental Studies of Water Seepage and Intermittent Flow in Unsaturated, Rough-Walled Fractures," *Water Resources Research*, Vol. 35, No. 4, April 1999, pp. 1019-1037.

Witherspoon, P.A., Wang, J.S.W., Iwai, K. and Gale, J.E., : Validity of cubic law for fluid flow in a deformable rock fracture, *Water Resources. Research.* Vol. 16, No. 6, 1980, pp 1016-1024.

Appendix A

A. Matlab Program for Saturation Measurement

```
% This program calculate the saturation of two-phase area.
% It is done by linear discriminant method.

clear;

% This part will ask user for the image to be processed.

File = input('\nEnter file name: ','s');
figure;
Image = imread(File);

% This will display the image and ask user to cut it to his desired dimension.

image(Image);
Sentinel = 0;
iter = 1;
FileNo = 1;

while (Sentinel ~= 1)
  Ymax = input('Enter y-axis maximum cutoff value: ');
 Ymin = input('Enter y-axis minimum cutoff value: ');
  Xmax = input('Enter x-axis maximum cutoff value: ');
  Xmin = input('Enter x-axis minimum cutoff value: ');
  cutImg = Image(Ymin:Ymax, Xmin:Xmax, :);
  figure;
  image(cutImg);
  text(3,5, File)
  Sentinel = input('Is this good? Enter 1 if yes, 2 for no: ');
  if(Sentinel == 2)
   close;
```

```
  end
end

[rImg,cImg]=size(cutImg);

sample = GenerateSample(cutImg);

%generation of phase data set
NtrnL=input('No. of liquid sample data: ');
liq = GetTrainingData(cutImg);
for i=1:(NtrnL-1)
  liqNew = GetTrainingData(cutImg);
  trnl=[liq;liqNew];
end

trl=CheckVariance(trnl);

Ntrng=input('No. of gas sample data: ');
gas = GetTrainingData(cutImg);
for i=1:(Ntrng-1)
  gasNew = GetTrainingData(cutImg);
  trng=[gas;gasNew];
end

trg=CheckVariance(trng);

Ntrnbk=input('No. of black strip data: ');
stp = GetTrainingData(cutImg);
for i=1:(Ntrnbk-1)
  stpNew = GetTrainingData(cutImg);
  trnstp=[stp;stpNew];
end

trstp=CheckVariance(trnstp);
trn =[trl;trg;trstp];

%generation of grouping
[RTr1,CTr1] = size(trnl);
```

```
[RTr2,CTr2] = size(trng);
[RTr3,CTr3] = size(trnstp);
grp1 = ones(RTr1,1);
grp2 = ones(RTr2,1).*2;
grp3 = ones(RTr3,1).*3;

grp=[grp1;grp2;grp3];

DoClassification(sample, trn, grp, File, rImg, cImg);

another =input('another? 1-yes, 2-no:' );
while (another ==1)
   close all;
   File = input('\nEnter file name: ','s');
   figure;
   Image = imread(File);
   image(Image);
   cutImg = Image(Ymin:Ymax, Xmin:Xmax, :);
   figure;
   image(cutImg);
   [rImg,cImg]=size(cutImg);
   sample = GenerateSample(cutImg);
   DoClassification(sample, trn, grp, File, rImg, cImg);
   another = input('another? 1-yes,2-no:' );
end

**********File Generate Sample**********
% This part will create the group based on the number of rows of tr1 and tr2
function sample = GenerateSample(cutImg)
red = double(cutImg(:,:,1));
green = double(cutImg(:,:,2));
blue = double(cutImg(:,:,3));
sample=[red(:),green(:),blue(:)];
GenerateSample = sample;
**********File GetTrainingData**********
function Trn = GetTrainingData(image)
% This function creates a matrix of training data using the polygon
% specified by the user
```

```
red = double(image(:,:,1));
green = double(image(:,:,2));
blue = double(image(:,:,3));

mask1=roipoly;
fprintf('Using this image, creat a polygon to represent the phase\n');
trn1r = red(mask1);
trn1g = green(mask1);
trn1b = blue(mask1);
Trn=[trn1r trn1g trn1b];
**********File CheckVariance**********
function trl = CheckVariance(trnl)

varl=var(trnl);
[row,col]=size(trnl);
err=0.001*rand(row,1);

if (varl(1,1)==0)
  trnl1=trnl(:,1)+err;
else
  trnl1=trnl(:,1);
end

if (varl(1,2)==0)
  trnl2=trnl(:,2)+err;
else
  trnl2=trnl(:,2);
end

if (varl(1,3)==0)
  trnl3=trnl(:,3)+err;
else
  trnl3=trnl(:,3);
end

trl=[trnl1 trnl2 trnl3];
**********File DoClassification**********
```

```
function DoClassification(sample, trn, grp, File, rImg,cImg)

class =classify(sample,trn,grp);
classImg =reshape(class,rImg,cImg/3);
figure;
imagesc(classImg);
colormap(gray);
Sw = sum(class==1)/(sum(class==1)+sum(class==2))
text(1,1,File, 'Color','r');
satString = num2Str(Sw);
satLabel = strcat('Sw=', satString)
xlabel(satLabel);
```

Appendix B

B. Calculations

Notes:

Runs 2, 3, and 4 were all done for smooth-walled fractures while runs 5,6, and 7 were for rough-walled fractures. All the calculations in the following tables use these constants:

Fracture length: 1 ft.

Fracture width: 0.33 ft

Nitrogen viscosity: 0.018cp

Water viscosity: 1 cp

Water density: 62.3 lb/ cu. ft

Nitrogen density: 0.0782 lb/cu. ft

				LIQUID PHASE					
Expt	Image File	Sw	delPl read Volts	Ql reading cc/min	delP act psi	qact cc/min	ql cu. ft /day	Kabskrl md	krl md
run2		1							1
Drainage		0.8904	1.192	8.55	0.598	8.506	0.433	1376088.249	0.587
		0.9215	0.952	8.55	0.478	8.506	0.433	1722420.113	0.735
	17h24.jpg	0.9073	1.132	8.55	0.568	8.506	0.433	1448923.007	0.618
	17h25.jpg	0.883	1.105	8.55	0.554	8.506	0.433	1484275.448	0.633
	17h26.jpg	0.883	0.907	8.55	0.455	8.506	0.433	1807726.214	0.771
	17h28.jpg	0.904	1.259	8.55	0.631	8.506	0.433	1302949.982	0.556
run3	10h53	0.8789	1.017	8.55	0.510	8.506	0.433	1612506.910	0.688
Drainage	11h00	0.8829	1.097	8.55	0.550	8.506	0.433	1495083.960	0.638
	11h54	0.7672	1.359	8.55	0.681	8.506	0.433	1207186.905	0.515
	11h59	0.7872	1.344	8.55	0.674	8.506	0.433	1220643.978	0.521
	12h14	0.7716	1.51	8.55	0.757	8.506	0.433	1086595.789	0.464
	12h29	0.7765	1.48	8.55	0.742	8.506	0.433	1108597.631	0.473
	14h40	0.7518	1.541	8.55	0.773	8.506	0.433	1064759.587	0.454
	12h58	0.7181	1.681	8.55	0.843	8.506	0.433	976166.595	0.416
	13h15	0.6965	1.659	8.55	0.832	8.506	0.433	989099.088	0.422
	13h35	0.6762	1.942	8.55	0.973	8.506	0.433	845080.046	0.361
	13h46	0.6545	1.898	8.55	0.951	8.506	0.433	864654.468	0.369
	14h05	0.6761	1.964	8.55	0.984	8.506	0.433	835621.466	0.357
	14h09	0.645	1.556	8.55	0.780	8.506	0.433	1054505.722	0.450
	14h10	0.6086	1.564	8.55	0.784	8.506	0.433	1049117.334	0.448
	14h14	0.6263	1.709	8.55	0.857	8.506	0.433	960188.163	0.410
	14h16	0.6725	1.866	8.55	0.935	8.506	0.433	879469.729	0.375
	14h17	0.5885	1.733	8.55	0.869	8.506	0.433	946902.939	0.404
	14h18	0.5932	1.936	8.55	0.970	8.506	0.433	847696.936	0.362
	14h44	0.6816	2.081	8.55	1.043	8.506	0.433	788676.382	0.336
	14h54	0.5967	1.751	8.55	0.878	8.506	0.433	937177.800	0.400
	15h17	0.6699	2.147	8.55	1.076	8.506	0.433	764450.047	0.326
	15h35	0.677	2.093	8.55	1.049	8.506	0.433	784158.036	0.335
	15h45	0.6713	1.915	8.55	0.960	8.506	0.433	856985.082	0.366
	16h18	0.6282	2.201	8.55	1.103	8.506	0.433	745708.401	0.318
	16h30	0.6342	2.562	8.55	1.284	8.506	0.433	640699.428	0.273
	17h01	0.5538	2.516	8.55	1.261	8.506	0.433	652405.896	0.278
	17h25	0.5036	2.388	8.55	1.197	8.506	0.433	687352.349	0.293
	17h38	0.5045	2.775	8.55	1.391	8.506	0.433	591549.712	0.252
	17h44	0.51125	2.437	8.55	1.221	8.506	0.433	673541.023	0.287
	18h31	0.4808	2.367	8.55	1.186	8.506	0.433	693446.420	0.296
	18h45	0.4855	2.873	8.55	1.440	8.506	0.433	571382.759	0.244
	18h46	0.4802	3.091	8.55	1.549	8.506	0.433	531105.469	0.227
	19h15	0.5475	2.631	8.55	1.318	8.506	0.433	623906.789	0.266
	19h30	0.6015	2.623	7	1.314	6.966	0.354	512535.236	0.219
	19h44	0.5684	2.515	7	1.260	6.966	0.354	534530.731	0.228
	19h59	0.6932	2.965	7	1.486	6.966	0.354	453448.335	0.193
	20h16	0.7312	2.32	6	1.163	5.973	0.304	496810.643	0.212
	20h31	0.722	2.654	6	1.330	5.973	0.304	434325.738	0.185
	20h53	0.714	1.825	4	0.915	3.987	0.203	421431.453	0.180
	21h23	0.732	2.106	3	1.055	2.993	0.152	274237.029	0.117
	21h53	0.673	2.281	2	1.143	2.000	0.102	169183.099	0.072
	21h57	0.4358	2.198	1	1.102	1.007	0.051	88367.332	0.038
	21h58	0.3271	1.978	1	0.991	1.007	0.051	98187.921	0.042
	22h27	0.3187	1.838	1	0.921	1.007	0.051	105660.376	0.045
	22h41	0.2992	1.772	1	0.888	1.007	0.051	109592.263	0.047
	23h08	0.2525	1.9	1	0.952	1.007	0.051	102215.407	0.044
	24h17	0.1286	1.633	0.5	0.819	0.510	0.026	60241.365	0.026
	24h19	0.1337	1.671	0.5	0.838	0.510	0.026	58872.732	0.025
	24h45	0.085	2.337	0.5	1.171	0.510	0.026	42106.597	0.018
	24h50	0.084	2.342	0.5	1.174	0.510	0.026	42016.764	0.018
	2h12	0.081	0.963	0	0.483	0.000	0.000	0.000	0.000

Gas Phase

Expt	Image File	qG reading cc/min	qg actual cc/min	qg cu. Ft/day	dPG read volts	P2 reading volts	delP actual psi	P2 actual psi	K krg md	krg uncalib md	krg calib md
run2											0
Drainage			0.7	0.035597	1.203	1.166	0.608	0.071	2003.224	0.0009	0.0008
			0.84	0.042717	1.092	1.184	0.553	0.071	2645.212	0.0011	0.0011
	17h24.jpg		0.6	0.030512	1.104	1.052	0.559	0.065	1869.149	0.0008	0.0008
	17h25.jpg		0.6	0.030512	1.238	1.205	0.626	0.072	1669.033	0.0007	0.0007
	17h26.jpg		0.6	0.030512	1.501	1.48	0.757	0.085	1379.217	0.0006	0.0006
	17h28.jpg		0.6	0.030512	1.063	1.013	0.538	0.063	1940.332	0.0008	0.0008
run3	10h53	-0.001	0.85	0.043225	1.121	1.008	0.567	0.063	2608.287	0.0011	0.0011
Drainage	11h00	-0.001	0.56	0.028478	1.176	1.01	0.595	0.063	1638.952	0.0007	0.0007
	11h54	2	3.6167	0.18392	1.467	2.329	0.740	0.126	8504.602	0.0036	0.0035
	11h59	2	3.6167	0.18392	1.477	1.805	0.745	0.101	8447.547	0.0036	0.0035
	12h14	3	5.1257	0.260658	1.655	1.38	0.834	0.081	10694.987	0.0046	0.0044
	12h29	3	5.1257	0.260658	1.645	1.865	0.829	0.104	10759.469	0.0046	0.0045
	14h40	5	8.1437	0.414133	1.757	1.266	0.885	0.075	16013.292	0.0068	0.0066
	12h58	5	8.1437	0.414133	1.813	2.59	0.913	0.138	15522.356	0.0066	0.0064
	13h15	8	12.6707	0.644345	1.781	2.615	0.897	0.139	24581.720	0.0105	0.0102
	13h35	10	15.6887	0.797819	1.873	2.492	0.943	0.133	28952.526	0.0124	0.0120
	13h46	9	14.1797	0.721082	1.97	2.334	0.992	0.126	24888.132	0.0106	0.0103
	14h05	12	18.7067	0.951294	2.065	1.277	1.039	0.076	31333.263	0.0134	0.0129
	14h09	13	20.2157	1.028031	1.695	1.917	0.854	0.106	41193.405	0.0176	0.0171
	14h10	12	18.7067	0.951294	1.66	2.528	0.837	0.135	38915.698	0.0166	0.0161
	14h14	12	18.7067	0.951294	1.734	2.929	0.874	0.154	37267.861	0.0159	0.0154
	14h16	12	18.7067	0.951294	2.067	1.632	1.040	0.093	31303.143	0.0134	0.0129
	14h17	12	18.7067	0.951294	1.892	0.889	0.953	0.057	34177.853	0.0146	0.0141
	14h18	11	17.1977	0.874557	2.014	2.489	1.014	0.133	29530.272	0.0126	0.0122
	14h44	15	23.2337	1.181506	2.258	2.301	1.136	0.124	35609.502	0.0152	0.0146
	14h54	22	33.7967	1.718667	1.773	3.391	0.893	0.176	65860.692	0.0281	0.0273
	15h17	22	33.7967	1.718667	2.292	3.332	1.153	0.173	51035.188	0.0218	0.0210
	15h35	22	33.7967	1.718667	2.249	2.565	1.131	0.137	52005.095	0.0222	0.0214
	15h45	27	41.3417	2.102354	2.003	3.99	1.008	0.204	71375.296	0.0305	0.0295
	16h18	40	60.9587	3.09994	2.505	2.842	1.259	0.150	84266.683	0.0360	0.0345
	16h30	37	56.4317	2.869728	2.761	2.721	1.387	0.144	70811.235	0.0302	0.0289
	17h01	45	68.5037	3.483626	2.691	1.34	1.352	0.079	88184.123	0.0376	0.0360
	17h25	48	73.0307	3.713839	2.334	3.96	1.174	0.203	108308.053	0.0462	0.0445
	17h38	46	70.0127	3.560364	3.06	1.246	1.537	0.074	79306.524	0.0338	0.0322
	17h44	54	82.0847	4.174263	2.715	2.097	1.364	0.115	104737.392	0.0447	0.0427
	18h31	66	100.1927	5.095111	2.463	0.349	1.238	0.032	140850.894	0.0601	0.0577
	18h45	76	115.2827	5.862484	3.055	2.145	1.534	0.117	130798.659	0.0558	0.0531
	18h46	64	97.1747	4.941636	3.31	1.629	1.662	0.092	101794.404	0.0434	0.0411
	19h15	98	148.4807	7.550706	2.527	3.382	1.270	0.175	203475.964	0.0868	0.0833
	19h30	92	139.4267	7.090282	2.959	0.195	1.486	0.025	163301.023	0.0697	0.0663
	19h44	98	148.4807	7.550706	2.818	2.78	1.416	0.147	182565.001	0.0779	0.0743
	19h59	101	153.0077	7.780918	3.194	2.185	1.604	0.119	166078.159	0.0709	0.0672
	20h16	115	174.1337	8.855241	2.406	3.701	1.210	0.191	250563.984	0.1069	0.1027
	20h31	109	165.0797	8.394817	2.962	2.979	1.488	0.156	193151.707	0.0824	0.0785
	20h53	145	219.4037	11.15736	2.181	2.096	1.097	0.115	348071.084	0.1485	0.1432
	21h23	171	258.6377	13.15253	2.477	2.314	1.245	0.125	361549.066	0.1542	0.1480
	21h53	198	299.3807	15.22444	2.696	2.441	1.355	0.131	384678.603	0.1641	0.1569
	21h57	223	337.1057	17.14287	2.723	2.109	1.368	0.115	428878.415	0.1830	0.1749
	21h58	230	347.6687	17.68004	2.433	2.091	1.223	0.114	494745.687	0.2111	0.2027
	22h27	242	365.7767	18.60088	2.342	1.952	1.178	0.108	540622.205	0.2306	0.2218
	22h41	244	368.7947	18.75436	2.349	1.495	1.181	0.086	543467.853	0.2319	0.2230
	23h08	283	427.6457	21.74712	2.509	2.482	1.261	0.133	590221.627	0.2518	0.2415
	24h17	329	497.0597	25.27703	2.334	3.285	1.174	0.171	737163.527	0.3145	0.3026
	24h19	329	497.0597	25.27703	2.341	3.615	1.177	0.186	734972.012	0.3136	0.3016
	24h45	398	601.1807	30.57191	3.1551	0.453	1.584	0.037	660546.423	0.2818	0.2674
	24h50	398	601.1807	30.57191	3.182	0.405	1.598	0.034	654986.061	0.2794	0.2651
	2h12	462	697.7567	35.4831	1.956	0.52	0.985	0.040	1233403.930	0.5262	0.5092

LIQUID PHASE

Expt	Image File	Sw	delPl read Volts	Ql reading cc/min	delP act psi	qact cc/min	ql cu. ft /day	Kabskrl md	krl md
Imbibition	21-22	0.223	2.06	0.5	1.03245	0.50995	0.02593	47764.12	0.0204
run4	21-22b	0.23	2.278	0.5	1.14162	0.50995	0.02593	43196.39	0.0184
	21-31	0.2473	2.198	0.5	1.10156	0.50995	0.02593	44767.46	0.0191
	21-34	0.2314	2.13	1	1.06750	1.00660	0.05119	91186.33	0.0389
	21-35	0.258	2.271	1	1.13812	1.00660	0.05119	85528.81	0.0365
	21-51	0.227	2.177	1	1.09104	1.00660	0.05119	89219.12	0.0381
	21-56	0.2367	2.466	1	1.23577	1.00660	0.05119	78769.96	0.0336
	22-26	0.2664	2.251	2	1.12810	1.99990	0.10170	171436.27	0.0731
	22-27	0.2624	2.154	2	1.07952	1.99990	0.10170	179150.75	0.0764
	23-32	0.36	2.769	4	1.38752	3.98650	0.20273	277841.02	0.1185
	23-33	0.357	2.955	4	1.48066	3.98650	0.20273	260362.00	0.1111
	23-43	0.369	3.189	5	1.59785	4.97980	0.25324	301382.42	0.1286
	24-06	0.417	3.498	6	1.75260	5.97310	0.30375	329579.14	0.1406
	24-06b	0.41	3.132	6	1.56931	5.97310	0.30375	368073.54	0.1570
	24-10	0.512	3.398	6	1.70252	5.97310	0.30375	339273.79	0.1447
	24-13	0.4894	3.727	6	1.86728	5.97310	0.30375	309337.31	0.1320
	24-14	0.516	3.738	6	1.87279	5.97310	0.30375	308427.40	0.1316
	24-35	0.5712	3.467	6.5	1.73707	6.46975	0.32901	360173.39	0.1537
	24-53	0.4855	3.055	6.5	1.53074	6.46975	0.32901	408721.30	0.1744
	1-13	0.4518	3.036	6.5	1.52123	6.46975	0.32901	411277.83	0.1755
	1-30	0.581	2.766	7.5	1.38601	7.46305	0.37952	520704.65	0.2222
	1-36	0.586	3.059	7.5	1.53275	7.46305	0.37952	470856.06	0.2009
	1-45	0.576	2.689	7.5	1.34745	7.46305	0.37952	535606.26	0.2285
	2-08	0.633	1.893	8	0.94881	7.95970	0.40478	811255.73	0.3461
	2-15	0.643	2.322	8	1.16366	7.95970	0.40478	661475.60	0.2822
	2-16	0.646	2.522	8	1.26382	7.95970	0.40478	609052.38	0.2598
	2-24	0.618	2.161	9	1.08303	8.95300	0.45529	799412.48	0.3411
	2-25	0.628	2.122	9	1.06350	8.95300	0.45529	814093.74	0.3473
	2-33	0.655	2.083	9	1.04397	8.95300	0.45529	829324.33	0.3538
	2-45	0.596	2.3	9.5	1.15264	9.44965	0.48054	792801.35	0.3382
	2-46	0.598	1.953	9.5	0.97886	9.44965	0.48054	933547.50	0.3983
	2-54	0.665	1.947	9.5	0.97586	9.44965	0.48054	936422.02	0.3995
	2-4b	0.659	1.898	9.5	0.95132	9.44965	0.48054	960576.97	0.4098
	2-56	0.631	1.898	9.5	0.95132	9.44965	0.48054	960576.97	0.4098
	2-58	0.614	2.214	9.5	1.10957	9.44965	0.48054	823574.50	0.3514
	3-05	0.679	1.378	9.5	0.69090	9.44965	0.48054	1322639.12	0.5643

Gas Phase

Expt	Image File	qG reading cc/min	qg actual cc/min	qg cu. Ft/day	dPG read volts	P2 reading volts	delP actual psi	P2 actual psi	K krg md	krg uncalib md	krg calib md
Imbibition	21-22	357	539.3117	27.42568	2.752	3.018	1.3827	0.1582	678938	0.2897	0.2768
run4	21-22b	357	539.3117	27.42568	3.017	3.18	1.5152	0.1659	619570	0.2643	0.2515
	21-31	356	537.8027	27.34894	2.83	3.91	1.4217	0.2005	658467	0.2809	0.2681
	21-34	356	537.8027	27.34894	2.791	3.001	1.4022	0.1574	667623	0.2848	0.2720
	21-35	357	539.3117	27.42568	2.906	3.734	1.4597	0.1921	643126	0.2744	0.2616
	21-51	357	539.3117	27.42568	2.892	3.603	1.4527	0.1859	646225	0.2757	0.2629
	21-56	360	543.839	27.656	3.14	3.515	1.5767	0.1818	600403	0.2562	0.2433
	22-26	335	506.114	25.737	2.889	5.1	1.4512	0.2568	607072	0.2590	0.2470
	22-27	319	481.970	24.510	2.821	3.862	1.4172	0.1982	591980	0.2526	0.2411
	23-32	283	427.646	21.747	3.268	0.37	1.6407	0.0328	453710	0.1936	0.1834
	23-33	268	405.011	20.596	3.443	3.054	1.7282	0.1599	407940	0.1740	0.1645
	23-43	261	394.448	20.059	3.801	4.11	1.9071	0.2099	360014	0.1536	0.1444
	24-06	206	311.453	15.838	4.113	0.334	2.0631	0.0311	262772	0.1121	0.1048
	24-06b	215	325.034	16.529	3.655	0.362	1.8342	0.0324	308466	0.1316	0.1239
	24-10	160	242.039	12.308	3.605	3.88	1.8092	0.1990	232875	0.0994	0.0937
	24-13	165	249.584	12.692	0.393	3.156	0.2033	0.1648	2137112	0.9118	0.9056
	24-14	160	242.039	12.308	3.79	5.2	1.9016	0.2616	221549	0.0945	0.0889
	24-35	103	156.026	7.934	3.671	0.357	1.8422	0.0322	147430	0.0629	0.0592
	24-53	108	163.571	8.318	2.964	3.939	1.4887	0.2018	191258	0.0816	0.0777
	1-13	103	156.026	7.934	3.231	3.275	1.6222	0.1704	167423	0.0714	0.0677
	1-30	80	121.319	6.169	3.044	2.738	1.5287	0.1450	138142	0.0589	0.0561
	1-36	76	115.283	5.862	3.173	3.135	1.5932	0.1638	125955	0.0537	0.0510
	1-45	71	107.738	5.479	2.961	2.803	1.4872	0.1480	126101	0.0538	0.0512
	2-08	51	77.558	3.944	1.967	2.754	0.9902	0.1457	136335	0.0582	0.0563
	2-15	55	83.594	4.251	2.423	2.644	1.2182	0.1405	119445	0.0510	0.0490
	2-16	52	79.067	4.021	2.699	2.398	1.3562	0.1289	101482	0.0433	0.0414
	2-24	29	44.360	2.256	2.283	2.165	1.1482	0.1178	67249	0.0287	0.0276
	2-25	30	45.869	2.333	2.057	3.036	1.0352	0.1591	77126	0.0329	0.0318
	2-33	30	45.869	2.333	2.087	2.425	1.0502	0.1301	76024	0.0324	0.0313
	2-45	10	15.689	0.798	2.32	1.435	1.1667	0.0832	23407	0.0100	0.0096
	2-46	9	14.180	0.721	1.977	2.807	0.9952	0.1482	24801	0.0106	0.0102
	2-54		8.89	0.452	1.942	1.736	0.9777	0.0975	15827	0.0068	0.0065
	2-4b		4.5	0.229	1.895	1.814	0.9542	0.1012	8209	0.0035	0.0034
	2-56		6.05	0.308	1.895	1.814	0.9542	0.1012	11036	0.0047	0.0046
	2-58		1.82	0.093	2.198	1.528	1.1057	0.0876	2865	0.0012	0.0012
	3-05		0	0	1.348	1.02	0.6807	0.0636	0	0.0000	0.0000

		Homogeneous Single Phase Approach				
		Dpave	NreM	Friction f	3.23/Nre^.75	dp Predicted
Expt	File					
run2		0.60300	1.91737	1.81514	1.98232	0.65854
		0.51516	1.94599	1.52746	1.96041	0.66118
	17h24.jpg	0.56323	1.89691	1.71407	1.99833	0.65664
	17h25.jpg	0.58997	1.89691	1.79543	1.99833	0.65664
	17h26.jpg	0.60613	1.89691	1.84463	1.99833	0.65664
	17h28.jpg	0.58478	1.89691	1.77965	1.99833	0.65664
run3	10h53	0.53868	1.94803	1.59550	1.95887	0.66137
	11h00	0.57247	1.88873	1.74987	2.00482	0.65587
	11h54	0.71081	2.51045	1.62417	1.61953	0.70878
	11h59	0.70956	2.51045	1.62130	1.61953	0.70878
	12h14	0.79562	2.81466	1.61635	1.48639	0.73165
	12h29	0.78561	2.81466	1.59601	1.48639	0.73165
	14h40	0.82888	3.41775	1.37807	1.28498	0.77289
	12h58	0.87794	3.41775	1.45963	1.28498	0.77289
	13h15	0.86443	4.30934	1.12919	1.07993	0.82672
	13h35	0.95829	4.89522	1.09517	0.98146	0.85880
	13h46	0.97152	4.60312	1.18440	1.02781	0.84307
	14h05	1.01179	5.47445	1.02762	0.90250	0.88860
	14h09	0.81714	5.76160	0.78614	0.86855	0.90280
	14h10	0.81039	5.47445	0.82307	0.90250	0.88860
	14h14	0.86520	5.47445	0.87873	0.90250	0.88860
	14h16	0.98776	5.47445	1.00320	0.90250	0.88860
	14h17	0.91071	5.47445	0.92495	0.90250	0.88860
	14h18	0.99203	5.18566	1.06693	0.93994	0.87395
	14h44	1.08934	6.33107	0.94794	0.80927	0.92999
	14h54	0.88546	8.27486	0.57723	0.66204	1.01555
	15h17	1.11436	8.27486	0.72645	0.66204	1.01555
	15h35	1.09009	8.27486	0.71063	0.66204	1.01555
	15h45	0.98403	9.61823	0.54379	0.59140	1.07019
	16h18	1.18113	12.94769	0.46704	0.47321	1.19675
	16h30	1.33552	12.19939	0.56527	0.49482	1.16907
	17h01	1.30650	14.16947	0.46548	0.44227	1.24135
	17h25	1.18521	14.88778	0.39856	0.42617	1.26730
	17h38	1.46360	14.41012	0.51132	0.43672	1.25006
	17h44	1.29272	16.29244	0.39075	0.39830	1.31770
	18h31	1.21220	18.98102	0.30457	0.35519	1.41369
	18h45	1.48689	21.10737	0.32732	0.32800	1.48997
	18h46	1.60522	18.54363	0.41501	0.36146	1.39807
	19h15	1.29430	25.45915	0.22360	0.28498	1.64963
	19h30	1.40029	23.00953	0.31575	0.30745	1.36346
	19h44	1.33800	24.05773	0.28368	0.29735	1.40244
	19h59	1.54467	24.57031	0.31798	0.29268	1.42177
	20h16	1.18618	25.53705	0.25075	0.28433	1.34502
	20h31	1.40880	24.64987	0.31415	0.29197	1.30933
	20h53	1.00599	25.02132	0.24909	0.28872	1.16601
	21h23	1.15034	23.66959	0.31240	0.30100	1.10833
	21h53	1.24891	20.20995	0.41121	0.33887	1.02920
	21h57	1.23487	14.25129	0.60220	0.44036	0.90302
	21h58	1.10729	14.44459	0.51881	0.43594	0.93042
	22h27	1.04949	14.77135	0.46020	0.42868	0.97761
	22h41	1.03471	14.82528	0.44886	0.42751	0.98551
	23h08	1.10676	15.85193	0.39437	0.40658	1.14100
	24h17	0.99616	12.44210	0.41624	0.48756	1.16685
	24h19	1.00742	12.44210	0.42095	0.48756	1.16685
	24h45	1.37770	14.00455	0.42685	0.44617	1.44006
	24h50	1.38567	14.00455	0.42932	0.44617	1.44006

Homogeneous Single Phase Approach

Expt	File	Dpave psi	NreM	Friction f	3.23/Nre^.75	dp Predicted psi
Imbibition	21-22	1.20757	13.07827	0.44430	0.46967	1.27650
run4	21-22b	1.32840	13.07827	0.48876	0.46967	1.27650
	21-31	1.26162	13.05560	0.46624	0.47028	1.27256
	21-34	1.23485	17.68264	0.32127	0.37458	1.43973
	21-35	1.29890	17.70713	0.33661	0.37419	1.44389
	21-51	1.27186	17.70713	0.32961	0.37419	1.44389
	21-56	1.40622	17.78052	0.36018	0.37303	1.45638
	22-26	1.28964	25.13572	0.22706	0.28773	1.63426
	22-27	1.24836	24.62945	0.23344	0.29215	1.56237
	23-32	1.51409	34.85008	0.18282	0.22519	1.86502
	23-33	1.60441	34.00072	0.20574	0.22940	1.78892
	23-43	1.75250	37.75596	0.18892	0.21206	1.96718
	24-06	1.90787	36.38536	0.22264	0.21803	1.86831
	24-06b	1.70173	37.25717	0.18993	0.21419	1.91908
	24-10	1.75584	31.43101	0.26589	0.24332	1.60682
	24-14	1.88722	31.43101	0.28578	0.24332	1.60682
	24-35	1.78961	24.34713	0.38951	0.29469	1.35398
	24-53	1.50971	25.14574	0.31356	0.28764	1.38493
	1-13	1.57170	24.34713	0.34208	0.29469	1.35398
	1-30	1.45735	21.20275	0.35031	0.32690	1.35993
	1-36	1.56296	20.41885	0.39457	0.33626	1.33201
	1-45	1.41732	19.41633	0.38171	0.34920	1.29662
	2-08	0.96952	15.35976	0.33171	0.41631	1.21678
	2-15	1.19093	16.27040	0.38024	0.39871	1.24876
	2-16	1.31000	15.58921	0.44033	0.41170	1.22484
	2-24	1.11562	10.27196	0.54759	0.56294	1.14689
	2-25	1.04936	10.53558	0.50079	0.55234	1.15739
	2-33	1.04709	10.53558	0.49970	0.55234	1.15739
	2-45	1.15967	5.10134	1.14845	0.95157	0.96086
	2-46	0.98704	4.80758	1.04012	0.99485	0.94408
	2-54	0.97679	3.76567	1.32714	1.19487	0.87944
	2-4b	0.95277	2.88634	1.70288	1.45862	0.81611
	2-56	0.95277	3.19835	1.53227	1.35054	0.83977

LIQUID PHASE

Expt	File	Sw	delPl read Volts	l reading cc/min	delP act psi	qact cc/min	ql cu. ft /day	kkrl md	krl md
run5	125008	0.86866	1.316	8.5	0.6599	8.4564	0.4300	1239305	0.6995
	125020	0.7724	1.257	8.5	0.6303	8.4564	0.4300	1297401	0.7323
	125038	0.5547	0.985	8.5	0.4941	8.4564	0.4300	1655088	0.9341
	125129	0.70226	2.23	8.5	1.1176	8.4564	0.4300	731720.3	0.4130
	125140	0.8639	1.324	8.5	0.6639	8.4564	0.4300	1231826	0.6952
	131247	0.5675	2.104	8.5	1.0545	8.4564	0.4300	775506.8	0.4377
	131256	0.715	2.31	8.5	1.1576	8.4564	0.4300	706396.9	0.3987
	131308	0.879	1.696	8.5	0.8502	8.4564	0.4300	961891.9	0.5429
	131323	0.7754	1.608	8.5	0.8061	8.4564	0.4300	1014480	0.5726
	131343	0.762	1.64	8.5	0.8221	8.4564	0.4300	994705	0.5614
	131403	0.5898	1.382	8.5	0.6929	8.4564	0.4300	1180188	0.6661
	132803	0.71498	1.921	8.5	0.9628	8.4564	0.4300	849322.5	0.4794
	132905	0.7155	1.778	8.5	0.8912	8.4564	0.4300	917570	0.5179
	141048	0.715	1.608	8.5	0.8061	8.4564	0.4300	1014480	0.5726
	141149	0.6105	1.725	8.5	0.8647	8.4564	0.4300	945735.9	0.5338
	141210	0.715	1.608	8.5	0.8061	8.4564	0.4300	1014480	0.5726
	141218	0.691	1.278	8.5	0.6408	8.4564	0.4300	1276109	0.7202
	141610	0.526	0.957	8.5	0.4801	8.4564	0.4300	1703432	0.9614
	141619	0.681	1.506	8.5	0.7550	8.4564	0.4300	1083118	0.6113
	141637	0.715	2.149	8.5	1.0770	8.4564	0.4300	759279.8	0.4285
	145050	0.753	1.62	8.5	0.8121	8.4564	0.4300	1006973	0.5683
	145132	0.766	1.597	8.5	0.8006	8.4564	0.4300	1021461	0.5765
	145542	0.453	0.874	8.5	0.4385	8.4564	0.4300	1864904	1.0526
	145551	0.576	1.082	8.5	0.5427	8.4564	0.4300	1506930	0.8505
	145558	0.78	1.567	8.5	0.7856	8.4564	0.4300	1040997	0.5875
	152952	0.531	1.341	8.5	0.6724	8.4564	0.4300	1216228	0.6864
	153005	0.728	1.735	8.5	0.8697	8.4564	0.4300	940290	0.5307
	153011	0.775	2.634	8.5	1.3199	8.4564	0.4300	619557.9	0.3497
	153014	0.623	2.726	8.5	1.3660	8.4564	0.4300	598660.6	0.3379
	153457	0.583	1.605	8.5	0.8046	8.4564	0.4300	1016375	0.5736
	153529	0.73	2.869	8.5	1.4376	8.4564	0.4300	568838.1	0.3211
path starts	160910	0.678	2.641	8.5	1.3234	8.4564	0.4300	617916.7	0.3488
	161513	0.6801	2.41	8.5	1.2077	8.4564	0.4300	677105.2	0.3822
	161717	0.684	2.523	8.5	1.2643	8.4564	0.4300	646798.2	0.3651
	173541	0.577	2.621	8.5	1.3134	8.4564	0.4300	622629	0.3514
	173641	0.5788	2.554	8.5	1.2798	8.4564	0.4300	638952.4	0.3606
	173717	0.581	2.548	8.5	1.2768	8.4564	0.4300	640456.1	0.3615
	173823	0.5885	2.683	8.5	1.3444	8.4564	0.4300	608249.6	0.3433
	174050	0.5242	2.587	8.5	1.2964	8.4564	0.4300	630806.9	0.3560
	174307	0.58746	2.654	8.5	1.3299	8.4564	0.4300	614891.8	0.3470
	181754	0.5926	2.92	8.5	1.4631	8.4564	0.4300	558908.3	0.3155
	181914	0.5869	2.865	8.5	1.4356	8.4564	0.4300	569631.8	0.3215
	182120	0.56727	2.881	8.5	1.4436	8.4564	0.4300	566470.1	0.3197
	182427	0.5644	2.887	8.5	1.4466	8.4564	0.4300	565293.4	0.3191
	185428	0.53	3.015	8.5	1.5107	8.4564	0.4300	541307	0.3055
	185527	0.5296	3.055	8.5	1.5307	8.4564	0.4300	534223.2	0.3015
	185732	0.5389	3.042	8.5	1.5242	8.4564	0.4300	536505	0.3028
	185809	0.55412	3.092	8.5	1.5493	8.4564	0.4300	527833.8	0.2979
	185915	0.5585	2.984	8.5	1.4952	8.4564	0.4300	546927.5	0.3087
	193125	0.5005	2.771	7	1.3885	6.9664	0.3543	485176.3	0.2738
	193242	0.5573	2.702	7	1.3540	6.9664	0.3543	497558.8	0.2808
	193412	0.4767	2.438	7	1.2218	6.9664	0.3543	551401.9	0.3112
	193519	0.5173	2.822	7	1.4141	6.9664	0.3543	476413.1	0.2689
	193619	0.4797	2.281	7	1.1431	6.9664	0.3543	589328	0.3326
	201116	0.513	2.323	6	1.1642	5.9731	0.3038	496169.5	0.2800
	201304	0.474	2.44	6	1.2228	5.9731	0.3038	472393.3	0.2666
	201529	0.473	2.634	6	1.3199	5.9731	0.3038	437621.6	0.2470
	201742	0.469	2.787	6	1.3965	5.9731	0.3038	413610.9	0.2334
	204350	0.45752	2.182	5	1.0935	4.9798	0.2532	440369.6	0.2485

LIQUID PHASE

Expt	File	Sw	dPl read Volts	Ql reading cc/min	delP act psi	qact cc/min	ql cu. ft /day	kkrl md	krl
run5	204512	0.464	2.178	5	1.0915	4.980	0.253	441178	0.2261
drainage	204820	0.456	2.403	5	1.2042	4.980	0.253	399896	0.2049
	221045	0.454	2.512	4.5	1.2588	4.483	0.228	344402	0.1765
	221223	0.4454	2.731	4.5	1.3685	4.483	0.228	316800	0.1623
	221727	0.45121	2.723	4.5	1.3645	4.483	0.228	317731	0.1628
	225040	0.416	2.314	3.5	1.1597	3.490	0.177	291019	0.1491
	225305	0.441	2.354	3.5	1.1797	3.490	0.177	286078	0.1466
	225517	0.4416	2.663	3.5	1.3344	3.490	0.177	252903	0.1296
	225805	0.4547	2.296	3.5	1.1506	3.490	0.177	293299	0.1503
	233209	0.392	2.276	3	1.1406	2.993	0.152	253768	0.1300
	233533	0.3965	2.497	3	1.2513	2.993	0.152	231322	0.1185
	233729	0.4045	2.595	3	1.3004	2.993	0.152	222592	0.1141
	234013	0.4112	2.536	3	1.2708	2.993	0.152	227767	0.1167
	240945	0.348	2.095	2	1.0500	2.000	0.102	184192	0.0944
	241043	0.3427	1.989	2	0.9969	2.000	0.102	194001	0.0994
	241209	0.3436	2.166	2	1.0855	2.000	0.102	178159	0.0913
	241338	0.3449	1.906	2	0.9553	2.000	0.102	202442	0.1037
	244335	0.2883	1.942	1	0.9734	1.007	0.051	100007	0.0512
	244422	0.2995	2.025	1	1.0149	1.007	0.051	95911	0.0491
	244635	0.3073	1.968	1	0.9864	1.007	0.051	98686	0.0506
	244717	0.3118	1.979	1	0.9919	1.007	0.051	98138	0.0503
	10935	0.252	1.771	0.5	0.8877	0.510	0.026	55551	0.0285
	11007	0.2659	1.8	0.5	0.9022	0.510	0.026	54657	0.0280
	11054	0.252	1.814	0.5	0.9093	0.510	0.026	54236	0.0278
		0.132				0			0.0000

Expt	File	qG reading cc/min	qg actual cc/min	qg cu. Ft/day	delPG read volts	P2 reading volts	Gas Phase delP actual psi	P2 actual psi	K krg	krg uncalib	krg calib
run5	125008	-1	0.70	0.04	1.244	1.001	0.629	0.063	1938	0.00099	0.00097
	125020	0	0.84	0.04	1.137	1.056	0.575	0.065	2542	0.00130	0.00128
	125038	0	0.60	0.03	1.145	1.106	0.579	0.068	1803	0.00092	0.00091
	125129	0	0.60	0.03	2.361	3.296	1.187	0.171	880	0.00045	0.00043
	125140	0	0.60	0.03	1.419	3.204	0.716	0.167	1458	0.00075	0.00073
	131247	-1	0.85	0.04	2.045	0.8	1.029	0.053	1438	0.00074	0.00071
	131256	3	5.13	0.26	2.324	0.498	1.169	0.039	7634	0.00391	0.00376
	131308	1	2.11	0.11	1.586	1.174	0.800	0.071	4588	0.00235	0.00229
	131323	1	2.11	0.11	1.397	3.739	0.705	0.192	5202	0.00267	0.00260
	131343	1	2.11	0.11	1.585	1.36	0.799	0.080	4590	0.00235	0.00229
	131403	0	0.60	0.03	1.321	1.172	0.667	0.071	1562	0.00080	0.00078
	132803	1	2.11	0.11	1.875	1.214	0.944	0.073	3886	0.00199	0.00193
	132905	0	0.60	0.03	1.826	0.891	0.920	0.057	1133	0.00058	0.00056
	141048	5	8.14	0.41	1.59	1.418	0.802	0.082	17681	0.00906	0.00882
	141149	7	11.16	0.57	1.663	2.87	0.838	0.151	23178	0.01188	0.01155
	141210	5	8.14	0.41	1.59	1.418	0.802	0.082	17681	0.00906	0.00882
	141218	3	5.13	0.26	1.299	2.282	0.656	0.123	13596	0.00697	0.00682
	141610	5	8.14	0.41	0.848	2.023	0.431	0.111	32908	0.01686	0.01662
	141619	3	5.13	0.26	1.511	2.282	0.762	0.123	11705	0.00600	0.00585
	141637	6	9.65	0.49	2.166	2.256	1.090	0.122	15419	0.00790	0.00762
	145050	9	14.18	0.72	1.638	1.518	0.826	0.087	29891	0.01532	0.01490
	145132	8	12.67	0.64	1.585	1.533	0.799	0.088	27596	0.01414	0.01377
	145542	10	15.69	0.80	0.788	1.503	0.401	0.086	68141	0.03669	0.03620
	145551	6	9.65	0.49	1.125	1.488	0.569	0.086	29516	0.01513	0.01484
	145558	7	11.16	0.57	1.541	3.137	0.777	0.164	24997	0.01281	0.01248
	152952	17	26.25	1.33	1.265	1.084	0.639	0.067	71483	0.03663	0.03585
	153005	12	18.71	0.95	1.958	2.531	0.986	0.135	33034	0.01693	0.01638
	153011	13	20.22	1.03	2.734	1.446	1.374	0.084	25616	0.01313	0.01254
	153014	14	21.72	1.10	2.705	1.408	1.359	0.082	27822	0.01426	0.01363
	153457	17	26.25	1.33	1.548	2.053	0.781	0.113	58528	0.02999	0.02922
	153529	13	20.22	1.03	2.964	1.864	1.489	0.104	23638	0.01211	0.01153
path starts	160910	26	39.83	2.03	2.574	1.674	1.294	0.095	53595	0.02746	0.02631
	161513	26	39.83	2.03	2.384	1.779	1.199	0.100	57842	0.02964	0.02849
	161717	26	39.83	2.03	2.448	1.454	1.231	0.084	56338	0.02887	0.02772
	173541	35	53.41	2.72	2.579	1.948	1.296	0.108	71729	0.03676	0.03522
	173641	35	53.41	2.72	2.429	1.49	1.221	0.086	76134	0.03901	0.03747
	173717	36	54.92	2.79	2.508	2.31	1.261	0.125	75832	0.03886	0.03727
	173823	35	53.41	2.72	2.616	1.974	1.315	0.109	70720	0.03624	0.03470
	174050	36	54.92	2.79	2.524	1.608	1.269	0.091	75354	0.03861	0.03703
	174307	34	51.90	2.64	2.594	3.113	1.304	0.163	69302	0.03551	0.03402
	181754	43	65.49	3.33	2.852	1.967	1.433	0.108	79563	0.04077	0.03889
	181914	43	65.49	3.33	2.792	2.863	1.403	0.151	81264	0.04164	0.03977
	182120	43	65.49	3.33	2.822	2.506	1.418	0.134	80405	0.04120	0.03932
	182427	42	63.98	3.25	2.788	2.62	1.401	0.139	79505	0.04074	0.03891
	185428	57	86.61	4.40	2.992	2.308	1.503	0.125	100329	0.05141	0.04893
	185527	58	88.12	4.48	3.075	1.743	1.544	0.098	99333	0.05090	0.04838
	185732	56	85.10	4.33	3.021	3.377	1.517	0.175	97639	0.05003	0.04761
	185809	60	91.14	4.63	3.038	2.375	1.526	0.128	103981	0.05328	0.05068
	185915	57	86.61	4.40	2.957	2.902	1.485	0.153	101511	0.05202	0.04954
	193125	66	100.19	5.10	2.698	3.23	1.356	0.168	128644	0.06592	0.06305
	193242	58	88.12	4.48	2.753	2.424	1.383	0.130	110895	0.05683	0.05429
	193412	61	92.65	4.71	2.434	2.284	1.224	0.123	131787	0.06753	0.06486
	193519	60	91.14	4.63	2.84	2.103	1.427	0.115	111196	0.05698	0.05436
	193619	66	100.19	5.10	2.236	2.417	1.125	0.130	155064	0.07946	0.07656
	201116	69	104.72	5.33	2.426	2.743	1.220	0.145	149448	0.07658	0.07356
	201304	69	104.72	5.33	2.465	2.586	1.239	0.138	147096	0.07538	0.07236
	201529	74	112.26	5.71	2.661	2.211	1.337	0.120	146138	0.07489	0.07165
	201742	67	101.70	5.17	2.886	1.675	1.450	0.095	122115	0.06258	0.05965
	204350	86	130.37	6.63	2.369	2.44	1.191	0.131	190509	0.09762	0.09385

Expt	File	qG reading cc/min	qg actual cc/min	qg cu. Ft/day	delPG read volts	P2 reading volts	Gas Phase delP actual psi	P2 actual psi	K krg	krg uncalib	krg calib
run5	204512	76	115.28	5.86	2.376	1.813	1.195	0.101	167965	0.0861	0.0827
drainage	204820	80	121.32	6.17	2.456	2.219	1.235	0.120	171033	0.0876	0.0841
	221045	90	136.41	6.94	2.453	2.151	1.233	0.117	192541	0.0987	0.0947
	221223	88	133.39	6.78	2.772	2.286	1.393	0.124	166719	0.0854	0.0816
	221727	85	128.86	6.55	2.775	1.69	1.394	0.095	160888	0.0824	0.0787
	225040	97	146.97	7.47	2.369	2.587	1.191	0.138	214764	0.1101	0.1058
	225305	86	130.37	6.63	2.573	3.135	1.293	0.164	175484	0.0899	0.0862
	225517	85	128.86	6.55	2.841	2.567	1.427	0.137	157168	0.0805	0.0768
	225805	91	137.92	7.01	2.345	2.395	1.179	0.129	203585	0.1043	0.1003
	233209	105	159.04	8.09	2.324	2.334	1.169	0.126	236879	0.1214	0.1168
	233533	107	162.06	8.24	2.456	2.715	1.235	0.144	228472	0.1171	0.1124
	233729	105	159.04	8.09	2.76	2.371	1.387	0.128	199642	0.1023	0.0977
	234013	106	160.55	8.16	2.72	2.501	1.367	0.134	204485	0.1048	0.1002
	240945	117	177.15	9.01	2.272	1.86	1.143	0.103	269851	0.1383	0.1331
	241043	121	183.19	9.32	2.126	2.058	1.070	0.113	298087	0.1528	0.1474
	241209	117	177.15	9.01	2.21	2.091	1.112	0.114	277375	0.1421	0.1370
	241338	118	178.66	9.09	2.119	2.214	1.066	0.120	291675	0.1495	0.1443
	244335	142	214.88	10.93	2.212	2.429	1.113	0.130	336141	0.1723	0.1660
	244422	142	214.88	10.93	2.175	2.1	1.094	0.115	341824	0.1752	0.1689
	244635	141	213.37	10.85	2.098	1.69	1.056	0.095	351800	0.1803	0.1741
	244717	142	214.88	10.93	2.161	1.95	1.087	0.108	344024	0.1763	0.1700
	10935	162	245.06	12.46	2.016	1.618	1.015	0.092	420374	0.2154	0.2083
	11007	163	246.57	12.54	2.043	1.63	1.028	0.092	417409	0.2139	0.2067
	11054	163	246.57	12.54	2.061	1.68	1.037	0.095	413788	0.2120	0.2049
		195	294.85	14.99	2.453	1.243	0.930	0.074	551872	0.2828	0.2742

Homogeneous Single Phase Model Calculation

Expt	File	Dpave psi	friction f	NreM	2.8/Nre^0.66	delP calc psi
run5	125008	0.6443	1.7897	1.7400	2.0055	0.7577
drainage	125020	0.6028	1.6491	1.7662	1.9859	0.7618
	125038	0.5367	1.5072	1.7214	2.0199	0.7548
	125129	1.1524	3.2364	1.7214	2.0199	0.7548
	125140	0.6901	1.9380	1.7214	2.0199	0.7548
	131247	1.0419	2.8473	1.7680	1.9845	0.7621
	131256	1.1632	2.1768	2.5587	1.5549	0.8720
	131308	0.8249	1.9857	2.0020	1.8283	0.7971
	131323	0.7557	1.8190	2.0020	1.8283	0.7971
	131343	0.8107	1.9514	2.0020	1.8283	0.7971
	131403	0.6801	1.9102	1.7211	2.0201	0.7548
	132803	0.9535	2.2952	2.0020	1.8283	0.7971
	132905	0.9055	2.5433	1.7211	2.0201	0.7548
	141048	0.8039	1.2304	3.1089	1.3673	0.9376
	141149	0.8515	1.1022	3.6527	1.2293	0.9967
	141210	0.8039	1.2304	3.1089	1.3673	0.9376
	141218	0.6485	1.2137	2.5587	1.5549	0.8720
	141610	0.4554	0.6970	3.1089	1.3673	0.9376
	141619	0.7586	1.4197	2.5587	1.5549	0.8720
	141637	1.0834	1.5196	3.3816	1.2935	0.9679
	145050	0.8189	0.9183	4.1902	1.1229	1.0509
	145132	0.7999	0.9613	3.9223	1.1729	1.0243
	145542	0.4196	0.4411	4.4567	1.0781	1.0765
	145551	0.5560	0.7798	3.3816	1.2935	0.9679
	145558	0.7814	1.0115	3.6527	1.2293	0.9967
	152952	0.6558	0.4788	6.2798	0.8597	1.2359
	153005	0.9277	0.8663	4.9850	1.0013	1.1252
	153011	1.3468	1.1912	5.2469	0.9680	1.1485
	153014	1.3626	1.1447	5.5073	0.9375	1.1712
	153457	0.7927	0.5787	6.2798	0.8597	1.2359
	153529	1.4631	1.2941	5.2469	0.9680	1.1485
		1.2960	0.6787	8.5213	0.7029	1.4086
	160910	1.3086	0.6852	8.5213	0.7029	1.4086
	161513	1.2032	0.6301	8.5213	0.7029	1.4086
	161717	1.2475	0.6533	8.5213	0.7029	1.4086
	173541	1.3048	0.5322	10.6557	0.6065	1.5604
	173641	1.2505	0.5101	10.6557	0.6065	1.5604
	173717	1.2688	0.5051	10.8866	0.5979	1.5763
	173823	1.3296	0.5423	10.6557	0.6065	1.5604
	174050	1.2825	0.5106	10.8866	0.5979	1.5763
	174307	1.3168	0.5507	10.4236	0.6153	1.5442
	181754	1.4479	0.4933	12.4698	0.5467	1.6840
	181914	1.4191	0.4835	12.4698	0.5467	1.6840
	182120	1.4306	0.4874	12.4698	0.5467	1.6840
	182427	1.4236	0.4952	12.2471	0.5532	1.6690
	185428	1.5067	0.3980	15.4717	0.4741	1.8837
	185527	1.5375	0.3997	15.6782	0.4700	1.8973
	185732	1.5207	0.4083	15.2641	0.4784	1.8700
	185809	1.5375	0.3874	16.0883	0.4621	1.9244
	185915	1.4902	0.3937	15.4717	0.4741	1.8837
	193125	1.3721	0.3883	16.4913	0.4546	1.6856
	193242	1.3686	0.4375	14.9732	0.4845	1.5907
	193412	1.2227	0.3728	15.5505	0.4726	1.6267
	193519	1.4204	0.4398	15.3591	0.4764	1.6148
	193619	1.1339	0.3209	16.4913	0.4546	1.6856

Homogeneous Single Phase Model Calculation

Expt	File	Dpave psi	friction f	NreM	2.8/Nre^0.66	delP calc psi
run5	201116	1.1919	0.3794	16.3643	0.4569	1.5064
drainage	201304	1.2310	0.3918	16.3643	0.4569	1.5064
	201529	1.3286	0.3953	17.2094	0.4420	1.5589
	201742	1.4231	0.4660	16.0190	0.4634	1.4852
	204350	1.1424	0.3530	18.0827	0.4278	1.4530
	204512	1.1431	0.3990	16.6238	0.4522	1.3597
	204820	1.2195	0.4047	17.2188	0.4418	1.3972
	221045	1.2460	0.4087	17.9854	0.4293	1.3735
	221223	1.3806	0.4631	17.7246	0.4335	1.3560
	221727	1.3793	0.4790	17.3268	0.4400	1.3297
	225040	1.1754	0.4573	17.1476	0.4430	1.1950
	225305	1.2364	0.5438	15.9459	0.4648	1.1091
	225517	1.3808	0.6145	15.8317	0.4670	1.1012
	225805	1.1649	0.4838	16.5043	0.4543	1.1482
	233209	1.1547	0.4801	16.8124	0.4488	1.1329
	233533	1.2430	0.5067	16.9883	0.4458	1.1475
	233729	1.3435	0.5586	16.8124	0.4488	1.1329
	234013	1.3188	0.5429	16.9006	0.4473	1.1402
	240945	1.0963	0.5923	14.6017	0.4926	0.9569
	241043	1.0333	0.5382	14.8345	0.4875	0.9822
	241209	1.0986	0.5936	14.6017	0.4926	0.9569
	241338	1.0108	0.5411	14.6605	0.4913	0.9632
	244335	1.0430	0.8143	10.7572	0.6027	0.8102
	244422	1.0546	0.8233	10.7572	0.6027	0.8102
	244635	1.0210	0.8039	10.7259	0.6038	0.8049
	244717	1.0395	0.8115	10.7572	0.6027	0.8102
	10935	0.9512	1.0192	7.7638	0.7474	0.7321
	11007	0.9652	1.0255	7.7866	0.7460	0.7369
	11054	0.9732	1.0340	7.7866	0.7460	0.7369

Homogeneous Single Phase Model Calculation

Expt	File	Dpave	friction f	NreM	6.5/Nre^.83	delP calc
run6	432	2.0267	0.5925	14.2109	0.7182	2.4565
imbibition	136	2.5708	0.3816	27.8902	0.4104	2.7647
	130	2.7359	0.4061	27.8902	0.4104	2.7647
	153	2.2681	0.3464	27.0090	0.4215	2.7593
	156	2.4432	0.3732	27.0090	0.4215	2.7593
	0156b	2.3757	0.3603	27.1239	0.4200	2.7689
	236	2.6334	0.4056	26.3339	0.4304	2.7948
	237	2.6359	0.4059	26.3339	0.4304	2.7948
	238	2.7310	0.4206	26.3339	0.4304	2.7948
	239	2.5708	0.3959	26.3339	0.4304	2.7948
	256	2.5608	0.4197	25.2924	0.4451	2.7159
	257	2.4382	0.3964	25.4247	0.4432	2.7258
	258	2.5984	0.4258	25.2924	0.4451	2.7159
	259	2.3607	0.3838	25.4247	0.4432	2.7258
	309	2.4082	0.4354	23.0322	0.4810	2.6604
	310	2.3282	0.4210	23.0322	0.4810	2.6604
	311	2.3857	0.4354	22.8800	0.4837	2.6501
	317	2.4358	0.4404	23.0322	0.4810	2.6604
	31651	2.5052	0.4530	23.0322	0.4810	2.6604
	31706	2.3983	0.4377	22.8800	0.4837	2.6501
	31708	2.4158	0.4368	23.0322	0.4810	2.6604
	31712	2.4658	0.4500	22.8800	0.4837	2.6501
	318	2.3082	0.4173	23.0322	0.4810	2.6604
	335	2.5183	0.5394	19.6987	0.5477	2.5569
	336	2.4533	0.5255	19.6987	0.5477	2.5569
	337	2.5258	0.5410	19.6987	0.5477	2.5569
	338	2.4107	0.5164	19.6987	0.5477	2.5569
	339	2.5033	0.5362	19.6987	0.5477	2.5569
	400	2.1531	0.5150	17.4316	0.6062	2.5343
	401	2.2982	0.5422	17.6235	0.6007	2.5461
	402	2.1706	0.5121	17.6235	0.6007	2.5461
	410	2.0760	0.4898	17.6235	0.6007	2.5461
	430	2.0753	0.6177	13.9971	0.7273	2.4434
	431	2.3407	0.6967	13.9971	0.7273	2.4434
	432	2.0267	0.5925	14.2109	0.7182	2.4565
	450	2.3357	0.8931	10.7977	0.9021	2.3592
	451	2.2657	0.8663	10.7977	0.9021	2.3592
	453	2.0948	0.7819	11.0311	0.8862	2.3743
	106	2.9336	0.4229	28.5857	0.4021	2.7894
	102	2.8360	0.4088	28.5857	0.4021	2.7894
	100	4.0244	0.6080	27.8863	0.4104	2.7169
	1258	3.4189	0.4818	28.9266	0.3981	2.8256
	1257	4.4547	0.6458	28.4996	0.4031	2.7803
	1228	2.9936	0.4712	27.2616	0.4182	2.6567
	1227	2.7234	0.4310	27.1957	0.4191	2.6481

Homogeneous Single Phase Model Calculation

Expt	File	Dpave	friction f	NreM	6.5/Nre^.83	delP calc
	1226	2.6433	0.4183	27.1957	0.4191	2.6481
surge	122409	2.3556	0.3788	26.9961	0.4216	2.6221
data	122411	2.6133	0.4271	26.7942	0.4243	2.5961
	122412	2.8285	0.4673	26.6581	0.4261	2.5788
	122413	3.1313	0.5202	26.5897	0.4270	2.5702
	1246	3.0136	0.4794	27.1294	0.4199	2.6394
	1217	2.3631	0.4855	23.3924	0.4749	2.3116
	1212	2.4707	0.5103	23.3399	0.4758	2.3033
	1206	2.4557	0.5045	23.3924	0.4749	2.3116
	1202	2.3356	0.4824	23.3399	0.4758	2.3033
	1139	2.0379	0.5949	18.6350	0.5735	1.9646
	1136	2.0379	0.5949	18.6350	0.5735	1.9646
	1134	2.0254	0.5913	18.6350	0.5735	1.9646
	1132	2.0253	0.5912	18.6350	0.5735	1.9646
	1058	1.6673	0.8368	12.4880	0.7995	1.5931
	1057	1.6758	0.8410	12.4880	0.7995	1.5931
	1055	1.6013	0.8036	12.4880	0.7995	1.5931
	1053	1.4439	0.7292	12.4617	0.8009	1.5859
	1012	1.4206	1.1103	8.6790	1.0814	1.3836
	1011	1.4186	1.1087	8.6790	1.0814	1.3836
	1010	1.4186	1.1087	8.6790	1.0814	1.3836
	1008	1.2005	0.9382	8.6790	1.0814	1.3836
	1002	1.5230	1.1903	8.6790	1.0814	1.3836
	942	1.3979	1.0925	8.6790	1.0814	1.3836
	940	1.4071	1.0997	8.6790	1.0814	1.3836
	935	1.1732	0.9169	8.6790	1.0814	1.3836
	4905	2.2855	1.7615	8.7227	1.0769	1.3973
run7	1022	2.6534	0.9904	11.0311	0.8862	2.3743
imbibition	1023	2.6910	0.9587	11.4943	0.8565	2.4040
	1024	2.7810	1.0380	11.0311	0.8862	2.3743
	1025	2.3707	0.8849	11.0311	0.8862	2.3743
	1028	1.9994	0.7289	11.2633	0.8710	2.3892
	1058	2.4858	1.6204	6.6430	1.3500	2.0711
	1059	2.2532	1.4688	6.6430	1.3500	2.0711
	1100	2.2832	1.4883	6.6430	1.3500	2.0711
	1102	2.0127	1.3120	6.6430	1.3500	2.0711
	1104	2.0710	1.3500	6.6430	1.3500	2.0711
	1147	2.0047	2.5909	3.3004	2.4127	1.8668
	1149	2.1098	2.9952	3.0135	2.6019	1.8327
	1150	2.0030	2.3838	3.5741	2.2583	1.8976
	1151	2.2183	3.1367	3.0253	2.5934	1.8341
	1154	2.1381	2.5445	3.5741	2.2583	1.8976
	1224	0.9077	1.8651	2.0028	3.6522	1.7775